


The optimum enhanced viscoelastic tuned mass dampers: Exact closed-form expressions

Journal of Vibration and Control
2023, Vol. 0(0) 1–23
© The Author(s) 2023
Article reuse guidelines:
sagepub.com/journals-permissions
DOI: 10.1177/10775463231156240
journals.sagepub.com/home/jvc


Sudip Chowdhury , Arnab Banerjee , and Sondipon Adhikari 

Abstract

This paper introduces the inertial amplifier viscoelastic tuned mass dampers (IAVTMD). The viscoelastic materials are implanted inside the core material of the inertial amplifier tuned mass dampers. The standard linear solid models are applied mathematically to formulate the viscoelastic material. H_2 and H_∞ optimization mechanisms apply to derive the exact mathematical closed-form formulations for optimal design parameters for novel inertial amplifier viscoelastic tuned mass dampers. The optimum IAVTMD installs at the top of the structures to mitigate the dynamic responses, determining the dynamic responses analytically through transfer function formation. At first, IAVTMD's dynamic response reduction capacity compares with the conventional tuned mass damper's (CTMD) dynamic response reduction capacity. As a result, H_2 optimized IAVTMD's dynamic response reduction capacity is significantly 20.87% and 26.47% superior to two well-established H_2 optimized conventional tuned mass damper's dynamic response reduction capacity. In addition, H_∞ optimized IAVTMD has 15.48% more dynamic response reduction capacity than H_∞ conventional tuned mass damper. H_2 and H_∞ optimized tuned mass damper inerters with optimal closed-form solutions are introduced in this paper. A higher damper mass ratio and a lower inverter mass ratio are recommended to produce H_2 and H_∞ optimized tuned mass damper inverter (TMDI) with a lower frequency and damping ratio in an affordable range. Accordingly, H_2 and H_∞ optimized IAVTMD's dynamic response reduction capacities are significantly 6.94% and 23.29% superior to H_2 and H_∞ optimized TMDI's dynamic response reduction capacity. The closed-form expressions for optimal design parameters of inertial amplifier viscoelastic tuned mass dampers and tuned mass damper inerters are mathematically correct and effective for practical applications.

Keywords

inertial amplifier viscoelastic tuned mass dampers, tuned mass damper inverter, conventional tuned mass dampers, standard linear solid, exact closed-form, H_2 and H_∞ optimization methods

Highlights

1. The inertial amplifier viscoelastic tuned mass dampers (IAVTMD) are introduced.
2. The new closed-form expressions for optimal design parameters of inertial amplifier viscoelastic tuned mass dampers (IAVTMD).
3. The H_2 and H_∞ optimization based closed-form expressions for optimal design parameters.
4. The inertial amplifier viscoelastic tuned mass dampers (IAVTMD) can enhance the vibration reduction performance by around 26% compared to conventional tuned mass dampers.

wind pressure through the storm, to protect the structures and living creatures. Tuned mass dampers are one of the prominent passive vibration control devices, controlling the dynamic responses of the structures and preventing structural damage during the above-mentioned vibratory events. In 1909, Frahm patented tuned mass dampers (TMD) (Frahm, 1909) without damping, resulting in vibration attenuation at only resonating frequency (Rana and Soong, 1998), that is, TMD's natural frequency close to the excitation frequency (Chowdhury et al., 2023a). However, the vibration attenuation performance

Introduction

Passive vibration control devices mitigate the dynamic response during natural calamities, such as earthquakes and high

Department of Civil Engineering, Indian Institute of Technology Delhi, India
Received: 29 September 2022; accepted: 23 January 2023

Corresponding author:

Sudip Chowdhury, Department of Civil Engineering, Indian Institute of Technology Delhi, Hauz Khas, New Delhi 110016, India.
Email: sudip.chowdhury@civil.iitd.ac.in

degrades at other frequency zones, such as minima and anti-resonance (Jimin and Zhi-Fang, 2001). To omit this drawback, system damping was provided by Ormondroyd and Den Hartog, deriving optimal design parameters in terms of closed-form expressions (Ormondroyd, 1928). The fixed-point theory was applied to derive these optimal closed-form solutions (Chowdhury and Banerjee, 2022b). However, later, J.P. Den Hartog thoroughly illustrated this optimization mechanism in his book (Den Hartog, 1985), namely “Mechanical Vibrations.” Later, H_∞ optimization nomenclature introduces to address the fixed-point theory (Baduidana and Kenfack-Jiotsa, 2021; Ćakmak et al., 2021; Chen and Hu, 2019a; Sun et al., 2019). Along with H_∞ optimization mechanism, another optimization method is concerned with deriving mathematical closed-form expressions for the damper’s optimal design parameters, called H_2 optimization, applicable for randomly excited dynamic systems (Adhikari et al., 2016; Chowdhury et al., 2022b; Khodaparast et al., 2008; Palmeri and Lombardo, 2011). An immense study was conducted on the TMD to mitigate the dynamic responses of automotive suspension systems, offshore platforms, buildings, and bridges with different solution procedures, analytical and numerical (Adhikari and Bhattacharya, 2012; Batou and Adhikari, 2019; Kasinos et al., 2021). The vibration reduction performance of TMD was amplified through a conventional approach, increasing the static mass of the damper, causing increasing the dead load, and affecting collapse during any seismic events with the presence of the damper. Therefore, to overcome this situation without affecting the static mass of the damper, recently, inerter (Smith, 2020) and inertial amplifiers (IA) Yilmaz et al., 2007) have started applying to the TMD to amplify the dampers’ effective mass, resulting in an increment in the dynamic response reduction capacity (Smith, 2020; Pietrosanti et al., 2017). Hence, the inerter-based (Petrini et al., 2020; Wagg, 2021) vibration absorbers (Chen and Hu, 2019b) are applied to mitigate the dynamic responses of the mechanical engineering machinery (De Domenico et al., 2019) and parts, notably automotive and train suspensions (Shen et al., 2016; Wang et al., 2006), buildings (Chowdhury et al., 2022b), wind turbines (Hu et al., 2018; Zhang and Fitzgerald, 2020; Zhang et al., 2019; Zhang and Høeg, 2021), and bridges (Song et al., 2021; Liang et al., 2021)). There are different types of inerter-inspired (Chowdhury and Banerjee, 2022a) TMD which were developed, such as tuned mass damper inerter (De Domenico and Ricciardi, 2018a; Su et al., 2022), tuned inerter damper (Shen et al., 2019; Wang et al., 2021), tuned viscous mass damper (Ma et al., 2021; Ikago et al., 2012), inerter-based dynamic vibration absorber (Hu and Chen, 2015), angular mass damper (Pradono et al., 2008), gyro-mass dampers (Hessabi and Mercan, 2016), rotational inertia viscous damper (Javidialesaadi and Wierschem, 2019a), viscous inertial mass damper (Lu et al., 2021), electromagnetic inertial mass dampers (Nakamura et al., 2014), rotational inertia dampers (Hwang et al., 2007), clutching inerter damper (Wang and Sun, 2018), tuned inertial mass electromagnetic transducers

(Asai et al., 2018), spring-dashpot-inerter (Basili et al., 2019), rotational inertial double tuned mass dampers (Javidialesaadi and Wierschem, 2018), tuned heave plate inerter (Ma et al., 2018), inerter-enhanced nonlinear energy sink (Javidialesaadi and Wierschem, 2019b), tuned liquid inerter system (Zhao et al., 2019b), tuned liquid column damper inerter (Di Matteo et al., 2022), shape memory alloy-tuned mass damper inerter (Tiwari et al., 2021), inerter-based isolators (Hu et al., 2015), inerter-based vibration isolation (Liu et al., 2022), friction pendulum inerter system (Zhao et al., 2019a), base-isolated structures via tuned mass damper and inerter devices (De Domenico and Ricciardi, 2018b), inerter-equipped vibrating barrier (Cacciola et al., 2020), nonlinear inerter-based vibration isolators (Yang et al., 2020), inerter-based isolator (De Souza Pippi et al., 2022), and full-scale hydraulic inerter-damper (Nakaminami et al., 2017) to mitigate the dynamic responses of structural systems (Marian and Giaralis, 2014). The effective mass amplifications, without affecting the static mass, of the dynamic systems have occurred through inertial amplifiers (IA) (Adhikari and Banerjee, 2021; Banerjee et al., 2021; Frandsen et al., 2016; Hussein et al., 2022; Phani and Hussein, 2017; Settini et al., 2021; Taniker and Yilmaz, 2013; Yilmaz and Hulbert, 2010), apart from the inerters. This effective mass amplification occurs through the generation of inertial forces through the rigid links, the amplifier’s mass, and the geometric configurations of the entire IA system (Adhikari and Banerjee, 2021; Banerjee et al., 2019, 2021). The inertial amplifiers (Frandsen et al., 2016) have been applied to the conventional base isolators and conventional TMD to increase their vibration reduction capacities without affecting the static mass of the entire system (Chowdhury et al., 2022b, 2023b), like inerters with different mass amplification mechanisms (Chowdhury et al., 2021, 2022b). These inertial amplifier-inspired passive vibration control devices (Chowdhury et al., 2022a) are installed in the single and multi-degree of freedom systems to mitigate the dynamic responses during vibratory situations (Chowdhury et al., 2022a, 2023a; Chowdhury and Banerjee, 2022b). Apart from the different structural configurations for enhancement of the vibration reduction performance, from the material perspective, the viscoelastic materials can also be applied to the traditional tuned mass damper to improve their dynamic response capacity (Batou and Adhikari, 2019). However, according to the existing literature review, best of the authors’ knowledge, the viscoelastic materials have not been implemented in the inertial amplifier-based TMD for enhancing their dynamic response reduction capacity. These could be the research scope for this paper.

Therefore, the optimum inertial amplifier viscoelastic tuned mass dampers (IAVTMD) are introduced in this paper. Additionally, the exact closed-form expressions for the optimal design parameters of IAVTMD have been introduced in this paper. H_2 and H_∞ optimization methods are applied to analytically derive these closed-form expressions (Chowdhury and Banerjee, 2022b). H_2 and H_∞ optimized tuned mass damper inerters with optimal closed-form solutions are also

introduced in this paper to make a fair comparison with optimum IAVTMD in mechanism and vibration control effectiveness. The dynamic response reduction capacity of optimum IAVTMD has been compared with the dynamic response reduction capacity of optimum conventional tuned mass dampers (CTMD) and tuned mass damper inerter (TMDI).

Structural model and equations of motion

The mathematical diagram of a single degree of freedom system controlled by inertial amplifier viscoelastic tuned mass dampers (IAVTMD) displays in Figure 1.

m_d and k_d represent the static mass and stiffness of IAVTMD. c_d and k_v represent the static hereditary damping and stiffness of the viscoelastic material, implanting inside the core material of inertial amplifier TMD. m_a and θ represent the mass and inertial angle of the inertial amplifier.

\ddot{x}_g notation denotes for the base excitation. The effective mass amplification characteristic of the IA is taken into consideration. Therefore, the static system properties, such as m_d and k_d are converted to m_{dv} and k_{dv} , representing effective mass and effective stiffness of the novel dampers. In addition, c_d and k_v are converted to c_{dv} and k_{av} , representing effective hereditary damping and stiffness of the viscoelastic material. These design parameters are also known as the loss factor and storage coefficient. m_s , k_s , and c_s refer to the mass, stiffness, and viscous damping of the primary structure. u_s and u_d refer to the absolute displacement of the primary structure and IAVTMD. x_a and y_a refer to the displacement of amplifier's mass m_a in x and y -directions. An inertial amplifier viscoelastic tuned mass damper with hereditary damping has been shown in Figure 1. Therefore, the equation of motion for the novel tuned mass damper derives as

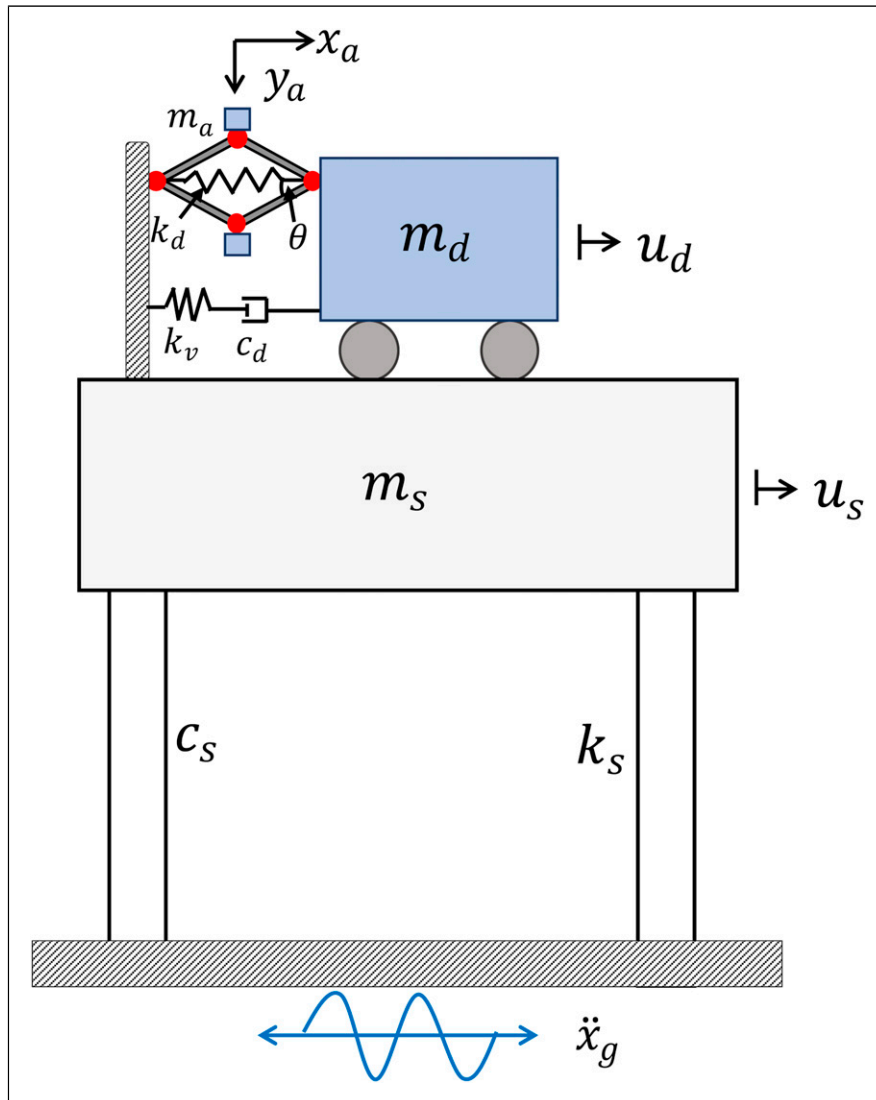


Figure 1. The schematic diagram of a single degree of freedom system equipped with IAVTMD subjected to base excitation.

$$m_{dv}\ddot{x}_d + \Xi \dot{x}_d + k_{dv}x_d = -m_{dv} \ddot{x}_g \quad (1)$$

where $x_d = u_d - u_s$ refers to the relative displacement of IAVTMD w.r.t primary structure. Ξ refers to the hereditary function and $\Xi \dot{x}_d$ has been solved by the convolution integral

$$\Xi \dot{x}_d = \int_{-\infty}^t \Xi(t-\tau) \dot{x}_d(\tau) d\tau \quad (2)$$

The novel tuned mass damper is in the static condition at $t = 0$. Therefore, equation (1) has been derived as

$$m_{dv}\ddot{x}_d + \int_{-\infty}^t \Xi(t-\tau) \dot{x}_d(\tau) d\tau + k_{dv}x_d = -m_{dv} \ddot{x}_g \quad (3)$$

The hereditary function Ξ has also been expressed as $\Xi(t) = k_{av}e^{-k_{av}t/c_{dv}}$ and the integrating form is a Dirac function at $k_{av} \rightarrow \infty$. The steady state solutions are considered as $x_d = X_d e^{i\omega t}$ and $\ddot{x}_g = A_g e^{i\omega t}$. Therefore, the transfer function of equation (3) has been derived as

$$X_d(\omega) = -\frac{m_{dv}}{[-\omega^2 m_{dv} + i\omega \Xi(\omega) + k_{dv}]} A_g \quad (4)$$

$\Xi(\omega) = k_{av}c_{dv}/(i\omega c_{dv} + k_{av})$ has been substituted in equation (4). Equation (4) has been expressed as

$$X_d(\omega) = -\frac{m_{dv}}{\left[-\omega^2 m_{dv} + \frac{i\omega k_{av}c_{dv}}{i\omega c_{dv} + k_{av}} + k_{dv}\right]} A_g \quad (5)$$

The derivation for effective system properties such as m_{dv} , c_{dv} , k_{dv} , and k_{av} has been listed below. The displacement responses of amplifier's mass m_a in x and y -directions are derived as

$$x_a = \frac{u_d + u_s}{2} \quad \text{and} \quad y_a = \pm \frac{u_d - u_s}{2\sin\theta} \quad (6)$$

The inertial forces developed through the amplifier's masses m_a in x and y -directions are derived as

$$p_x = m_a \ddot{x}_a \quad \text{and} \quad p_y = m_a \ddot{y}_a \quad (7)$$

The internal forces generated through the rigid links have been derived as

$$p_1 = \frac{1}{2} \left(\frac{p_y}{\sin\theta} - \frac{p_x}{\cos\theta} \right) \quad \text{and} \quad p_2 = \frac{1}{2} \left(\frac{p_y}{\sin\theta} + \frac{p_x}{\cos\theta} \right) \quad (8)$$

The resultant forces are generated towards the mass of the novel TMD which increases the effective property of the novel dampers. Therefore, the resultant forces are derived as

$$F = 2p_2 \cos\theta + k_d(u_d - u_s) \\ = \underbrace{\frac{0.5m_a}{\tan^2\theta}}_{c_1} (\ddot{u}_d - \ddot{u}_s) + \underbrace{0.5m_a}_{c_2} (\ddot{u}_d + \ddot{u}_s) + k_{dv}(u_d - u_s) \quad (9)$$

where $c_1 = (0.5m_a/\tan^2\theta)$ and $c_2 = 0.5m_a$ are the components of effective mass which have been added to the static mass of the novel tuned mass damper m_d . Hence, the effective mass of IAVTMD has been derived as

$$m_{dv} = m_d + 0.5m_a \left(1 + \frac{1}{\tan^2\theta} \right) \quad (10)$$

The effective stiffness of IAVTMD has been derived as

$$k_{dv} = m_{dv}\omega_d^2 \quad (11)$$

The effective damping of IAVTMD has been derived as

$$c_{dv} = 2\zeta_d m_{dv}\omega_d \quad (12)$$

The effective stiffness of viscoelastic material has been derived as

$$k_{av} = \alpha k_{dv} \quad (13)$$

where $\alpha = k_{av}/k_{dv}$ refers to the stiffness ratio of the damper to the viscoelastic material. The equations of motion of the main structure isolated by IAVTMD subjected to base excitations have been derived and expressed as

$$m_{dv}\ddot{x}_d + \int_{-\infty}^t \Xi(t-\tau) \dot{x}_d(\tau) d\tau + k_{dv}x_d + m_{dv}\ddot{x}_s = -m_{dv}\ddot{x}_g \\ m_s\ddot{x}_s + c_s\dot{x}_s + k_sx_s - \int_{-\infty}^t \Xi(t-\tau) \dot{x}_d(\tau) d\tau - k_{dv}x_d = -m_s\ddot{x}_g \quad (14)$$

Equation (14) has also been derived as

$$m_{dv}\ddot{x}_d + \int_0^\infty k_{av}e^{-(k_{av}/c_{dv})(t-\tau)} \dot{x}_d(\tau) d\tau + k_{dv}x_d + m_{dv}\ddot{x}_s \\ = -m_{dv}\ddot{x}_g \\ m_s\ddot{x}_s + c_s\dot{x}_s + k_sx_s - \int_0^\infty k_{av}e^{-(k_{av}/c_{dv})(t-\tau)} \dot{x}_d(\tau) d\tau - k_{dv}x_d \\ = -m_s\ddot{x}_g \quad (15)$$

where $x_d = u_d - u_s$ and $x_s = u_s - x_g$. The steady-state solutions for dynamic responses of controlled structures are derived as $x_s = X_s e^{i\omega t}$, $x_d = X_d e^{i\omega t}$, and $\ddot{x}_g = A_g e^{i\omega t}$. The viscous damping ratio of IAVTMD has been defined as $\zeta_d = c_{dv}/2\omega_d m_{dv}$. The natural frequency of IAVTMD defines as $\omega_d = \sqrt{k_{dv}/m_{dv}}$. The ratio of damper mass to the main structural mass defines as $\mu_d = m_d/m_s$. The ratio of amplifier mass to the main structural mass defines as $\mu_a = m_a/m_s$. The ratio of effective mass to main structural mass defines as $\mu_{dv} = m_{dv}/m_s$. η_b defines the ratio of damper frequency to the main structure's frequency. The stiffness of the main structure defines as $k_s = \omega_s^2 m_s$. The viscous damping ratio of main structure defines as $\zeta_s = c_s/2m_s\omega_s$. The steady state solutions and the design parameters are substituted in equations (14) and (15). Therefore, the transfer function has been derived as

$$\begin{bmatrix} 2\zeta_s q \omega_s + q^2 + \omega_s^2 & -2 \frac{q \alpha \omega_d^3 \mu_{dv}^2 \zeta_d}{\alpha \omega_d^2 \mu_{dv} + 2 \mu_{dv} q \omega_d \zeta_d} - \omega_d^2 \mu_{dv} \\ \mu_{dv} q^2 & \mu_{dv} q^2 + 2 \frac{q \alpha \omega_d^3 \mu_{dv}^2 \zeta_d}{\alpha \omega_d^2 \mu_{dv} + 2 \mu_{dv} q \omega_d \zeta_d} + \omega_d^2 \mu_{dv} \end{bmatrix} \begin{Bmatrix} X_s \\ X_d \end{Bmatrix} = - \begin{bmatrix} 1 \\ \mu_{dv} \end{bmatrix} A_g \quad (16)$$

where $q = i\omega$. The dynamic response of the primary structure derives as

$$H_s(q) = \frac{X_s}{A_g} = \frac{-2 \alpha \mu_{dv} q \omega_d^2 \zeta_d - \omega_d^3 \alpha \mu_{dv} - 2 \alpha q \omega_d^2 \zeta_d}{-2 \mu_{dv} q \omega_d^2 \zeta_d - \alpha q^2 \omega_d - \omega_d^3 \alpha - 2 q^3 \zeta_d - 2 \omega_d^2 \zeta_d q} \quad (17)$$

The dynamic response of IAVTMD derives as

$$H_d(q) = \frac{X_d}{A_g} = \frac{-(\alpha \omega_d + 2 q \zeta_d) \omega_s (2 q \zeta_s + \omega_s)}{\Delta} \quad (18)$$

Δ has been derived as

$$\begin{aligned} \Delta = & 2 \alpha \mu_{dv} q^3 \omega_d^2 \zeta_d + 4 \alpha q^2 \omega_d^2 \zeta_d \zeta_s \omega_s + \alpha \mu_{dv} q^2 \omega_d^3 + 2 \alpha q^3 \omega_d^2 \zeta_d + 2 \alpha q^3 \omega_d \zeta_s \omega_s \\ & + 2 \alpha q \omega_d^3 \zeta_s \omega_s + 2 \alpha q \omega_d^2 \zeta_d \omega_s^2 + 2 \mu_{dv} q^3 \omega_d^2 \zeta_d + 4 q^4 \zeta_d \zeta_s \omega_s + 4 q^2 \omega_d^2 \zeta_d \zeta_s \omega_s \\ & + \alpha q^4 \omega_d + \alpha q^2 \omega_d^3 + \alpha q^2 \omega_d \omega_s^2 + \alpha \omega_d^3 \omega_s^2 + 2 q^5 \zeta_d + 2 q^3 \omega_d^2 \zeta_d + 2 q^3 \zeta_d \omega_s^2 \\ & + 2 q \omega_d^2 \zeta_d \omega_s^2 \end{aligned} \quad (19)$$

Equations (17) and (19) are applied to derive the standard deviation and corresponding closed-form expressions for optimal design parameters of IAVTMD.

$$\sigma_{x_s, d}^2 = \int_{-\infty}^{\infty} \frac{\Xi_n(\omega) d\omega}{\Lambda_n(i\omega) \Lambda_n^*(i\omega)} = \frac{\pi}{u_4} \frac{\det[\mathbf{N}_4]}{\det[\mathbf{D}_4]} \quad (20)$$

H_2 optimization for IAVTMD

H_2 optimization method has been applied to derive the closed-form expressions for optimal design parameters for IAVTMD (Chowdhury and Banerjee, 2022b; Chowdhury et al., 2022b) subjected to random-white noise excitations. The viscous damping ratio of the primary structure considers as $\zeta_s = 0$. A mathematical equation has been derived to determine the standard deviation of the dynamic responses of the controlled structures and expressed as

$$N_4 = \begin{bmatrix} v_3 & v_2 & v_1 & v_0 \\ -u_4 & u_2 & -u_0 & 0 \\ 0 & -u_3 & u_1 & 0 \\ 0 & u_4 & -u_2 & u_0 \end{bmatrix} \quad \text{and} \quad D_4 = \begin{bmatrix} u_3 & -u_1 & 0 & 0 \\ -u_4 & u_2 & -u_0 & 0 \\ 0 & -u_3 & u_1 & 0 \\ 0 & u_4 & -u_2 & u_0 \end{bmatrix} \quad (21)$$

The standard deviation of the dynamic response of the primary structure has been derived as

$$\sigma_{x_s}^2 = \frac{S_0 \pi \left(\begin{aligned} & 4 \alpha^2 \mu_{dv}^3 \omega_d^4 \zeta_d^2 \omega_s^2 + \alpha^2 \mu_{dv}^4 \omega_d^6 + 12 \alpha^2 \mu_{dv}^2 \omega_d^4 \zeta_d^2 \omega_s^2 + 8 \alpha \mu_{dv}^3 \omega_d^4 \zeta_d^2 \omega_s^2 \\ & + 4 \alpha^2 \mu_{dv}^3 \omega_d^6 + \alpha^2 \mu_{dv}^3 \omega_d^4 \omega_s^2 + 12 \alpha^2 \mu_{dv} \omega_d^4 \zeta_d^2 \omega_s^2 + 24 \alpha \mu_{dv}^2 \omega_d^4 \zeta_d^2 \omega_s^2 \\ & + 4 \alpha^2 \omega_d^4 \zeta_d^2 \omega_s^2 + 24 \alpha \mu_{dv} \omega_d^4 \zeta_d^2 \omega_s^2 - 8 \alpha \mu_{dv} \omega_d^2 \zeta_d^2 \omega_s^4 + 12 \mu_{dv}^2 \omega_d^4 \zeta_d^2 \omega_s^2 \\ & + 4 \alpha^2 \mu_{dv} \omega_d^6 - 3 \alpha^2 \mu_{dv} \omega_d^4 \omega_s^2 + 8 \alpha \omega_d^4 \zeta_d^2 \omega_s^2 - 8 \alpha \omega_d^2 \zeta_d^2 \omega_s^4 \\ & + 4 \mu_{dv}^3 \omega_d^4 \zeta_d^2 \omega_s^2 + 12 \mu_{dv} \omega_d^4 \zeta_d^2 \omega_s^2 - 8 \mu_{dv} \omega_d^2 \zeta_d^2 \omega_s^4 + \alpha^2 \omega_d^6 - 2 \alpha^2 \omega_d^4 \omega_s^2 \\ & + \alpha^2 \omega_d^2 \omega_s^4 + 4 \omega_d^4 \zeta_d^2 \omega_s^2 - 8 \omega_d^2 \zeta_d^2 \omega_s^4 + 4 \zeta_d^2 \omega_s^6 + 6 \alpha^2 \mu_{dv}^2 \omega_d^6 \end{aligned} \right)}{2 \alpha^2 \omega_d^3 \zeta_d \mu_{dv} \omega_s^6} \quad (22)$$

Equation (22) has been partially differentiated with respect to the viscous damping ratio ζ_d and natural frequency ω_d of IAVTMD. Therefore, the mathematical

Equation (22) has been substituted in the first equation of equation (23). As a result, the closed-form expression for the viscous damping ratio of IAVTMD has been derived as

$$(\zeta_d)_{opt} = \sqrt{\frac{\alpha^2 \mu_{dv}^4 \omega_d^6 + 4 \alpha^2 \mu_{dv}^3 \omega_d^6 + \alpha^2 \mu_{dv}^3 \omega_d^4 \omega_s^2 + 6 \alpha^2 \mu_{dv}^2 \omega_d^6 + 4 \alpha^2 \mu_{dv} \omega_d^6 - 3 \alpha^2 \mu_{dv} \omega_d^4 \omega_s^2 + \alpha^2 \omega_d^6 - 2 \alpha^2 \omega_d^4 \omega_s^2 + \alpha^2 \omega_d^2 \omega_s^4}{4 \alpha^2 \mu_{dv}^3 \omega_d^4 \omega_s^2 + 12 \alpha^2 \mu_{dv}^2 \omega_d^4 \omega_s^2 + 8 \alpha \mu_{dv}^3 \omega_d^4 \omega_s^2 + 12 \alpha^2 \mu_{dv} \omega_d^4 \omega_s^2 + 24 \alpha \mu_{dv}^2 \omega_d^4 \omega_s^2 + 4 \mu_{dv}^3 \omega_d^4 \omega_s^2 + 4 \alpha^2 \omega_d^4 \omega_s^2 + 24 \alpha \mu_{dv} \omega_d^4 \omega_s^2 - 8 \alpha \mu_{dv} \omega_d^2 \omega_s^4 + 12 \mu_{dv}^2 \omega_d^4 \omega_s^2 + 4 \omega_s^6 + 8 \alpha \omega_d^4 \omega_s^2 - 8 \omega_d^2 \omega_s^4 - 8 \alpha \omega_d^2 \omega_s^4 + 12 \mu_{dv} \omega_d^4 \omega_s^2 - 8 \mu_{dv} \omega_d^2 \omega_s^4 + 4 \omega_d^4 \omega_s^2}} \quad (24)$$

equations for partial differentiation have been derived as

$$\frac{\partial \sigma_{x_s}^2}{\partial \zeta_d} = 0 \quad \text{and} \quad \frac{\partial \sigma_{x_s}^2}{\partial \omega_d} = 0 \quad (23)$$

The optimal frequency of IAVTMD needs to be separated from equation (24) to achieve the exact closed-form expression for IAVTMD. To perform that, equation (24) has been substituted in equation (22). The modified SD substitutes in the second equation of equation (23). Hence, the closed-form expression for the optimal frequency of IAVTMD has been derived as

$$\begin{aligned} A\omega_d^6 + B\omega_d^4 + C\omega_d^2 + E &= 0 \\ \omega_{d1}^2 &= \frac{\sqrt[3]{-108EA^2 + 36ABC + 12\sqrt{3}V_1A - 8B^3}}{6A} \\ &\quad - \frac{2(3AC - B^2)}{3A\sqrt[3]{-108EA^2 + 36ABC + 12\sqrt{3}V_1A - 8B^3}} - \frac{B}{3A} \\ \omega_{d2}^2 &= -\frac{\sqrt[3]{-108EA^2 + 36ABC + 12\sqrt{3}V_1A - 8B^3}}{12A} \\ &\quad + \frac{3AC - B^2}{3A\sqrt[3]{-108EA^2 + 36ABC + 12\sqrt{3}V_1A - 8B^3}} - \frac{B}{3A} \\ &\quad + \frac{1}{2} \left(i\sqrt{3} \left(\frac{\sqrt[3]{-108EA^2 + 36ABC + 12\sqrt{3}V_1A - 8B^3}}{6A} + \frac{2(3AC - B^2)}{3A\sqrt[3]{-108EA^2 + 36ABC + 12\sqrt{3}V_1A - 8B^3}} \right) \right) \\ \omega_{d3}^2 &= -\frac{\sqrt[3]{-108EA^2 + 36ABC + 12\sqrt{3}V_1A - 8B^3}}{12A} \\ &\quad + \frac{3AC - B^2}{3A\sqrt[3]{-108EA^2 + 36ABC + 12\sqrt{3}V_1A - 8B^3}} - \frac{B}{3A} \\ &\quad - \frac{1}{2} \left(i\sqrt{3} \left(\frac{\sqrt[3]{-108EA^2 + 36ABC + 12\sqrt{3}V_1A - 8B^3}}{6A} + \frac{2(3AC - B^2)}{3A\sqrt[3]{-108EA^2 + 36ABC + 12\sqrt{3}V_1A - 8B^3}} \right) \right) \end{aligned} \quad (25)$$

where

$$V_1 = \sqrt{27A^2E^2 - 18ABCE + 4AC^3 + 4B^3E - B^2C^2} \quad (26)$$

where the closed-form expressions for A , B , C , and E have been derived as

$$\begin{aligned} A &= 3 \alpha^2 \mu_{dv}^4 + 12 \alpha^2 \mu_{dv}^3 + 18 \alpha^2 \mu_{dv}^2 + 12 \alpha^2 \mu_{dv} + 3 \alpha^2 \\ &\quad 5 \alpha^2 \mu_{dv}^3 \omega_s^2 + 12 \alpha^2 \mu_{dv}^2 \omega_s^2 + 8 \alpha \mu_{dv}^3 \omega_s^2 \\ B &= +9 \alpha^2 \mu_{dv} \omega_s^2 + 24 \alpha \mu_{dv}^2 \omega_s^2 + 4 \mu_{dv}^3 \omega_s^2 \\ &\quad + 2 \alpha^2 \omega_s^2 + 24 \alpha \mu_{dv} \omega_s^2 + 12 \mu_{dv}^2 \omega_s^2 \\ &\quad + 8 \alpha \omega_s^2 + 12 \mu_{dv} \omega_s^2 + 4 \omega_s^2 \\ C &= -\alpha^2 \omega_s^4 + 8 \alpha \mu_{dv} \omega_s^4 + 8 \alpha \omega_s^4 + 8 \mu_{dv} \omega_s^4 + 8 \omega_s^4 \\ E &= -12 \omega_s^6 \end{aligned} \quad (27)$$

Equation (25) has been substituted in equation (24) to derive the optimal viscous damping ratio for IAVTMD. The second equation of equation (25) provides the optimal frequency ratio for IAVTMD. Therefore, the optimal closed-form expression for the optimal frequency of IAVTMD has been derived as

$$\omega_{d1}^2 = \frac{\sqrt[3]{-108 EA^2 + 36 ABC + 12 \sqrt{3} V_1 A - 8 B^3}}{6A} - \frac{2(3 AC - B^2)}{3A \sqrt[3]{-108 EA^2 + 36 ABC + 12 \sqrt{3} V_1 A - 8 B^3}} - \frac{B}{3A} \quad (28)$$

The variations of the optimal frequency ratio of IAVTMD versus damper mass ratio for the different values of inertial angles are shown in Figure 2(a). The system parameters are considered as $\mu_a = 0.01$ and $\alpha = 1.0$. The optimal frequency ratio of IAVTMD decreases as the inertial angle decreases.

The variations of the optimal frequency ratio of IAVTMD versus damper mass ratio for the different values of the amplifier's mass ratio are shown in Figure 2(b). The system parameters are considered as $\theta = 10^\circ$ and $\alpha = 1.0$. The optimal frequency ratio decreases as the damper mass ratio and amplifier's mass ratio increase. As a result, a higher damper mass ratio, a higher amplifier's mass ratio, and a lower inertial angle are recommended for H_2 optimized IAVTMD for achieving a lower frequency ratio without reducing the static mass of the entire system. The variations of optimal viscous damping ratio of IAVTMD versus damper mass ratio for the different values of inertial angles are shown in Figure 3(a). The system parameters are considered as $\mu_a = 0.01$ and $\alpha = 1.0$. The optimal viscous damping ratio of IAVTMD decreases as the inertial angle decreases.

The variations of the optimal viscous damping ratio of IAVTMD versus damper mass ratio for the different values of the amplifier's mass ratio are shown in Figure 3(b). The system parameters are considered as $\theta = 10^\circ$ and $\alpha = 1.0$. The optimal viscous damping ratio decreases as the damper mass ratio increases and decreases as the amplifier's mass ratio increases. As a result, a higher damper mass ratio, a moderate amplifier's mass ratio, and a lower inertial angle are recommended for H_2 optimized IAVTMD to achieve an average viscous damping ratio without reducing the static mass of the entire controlled structure.

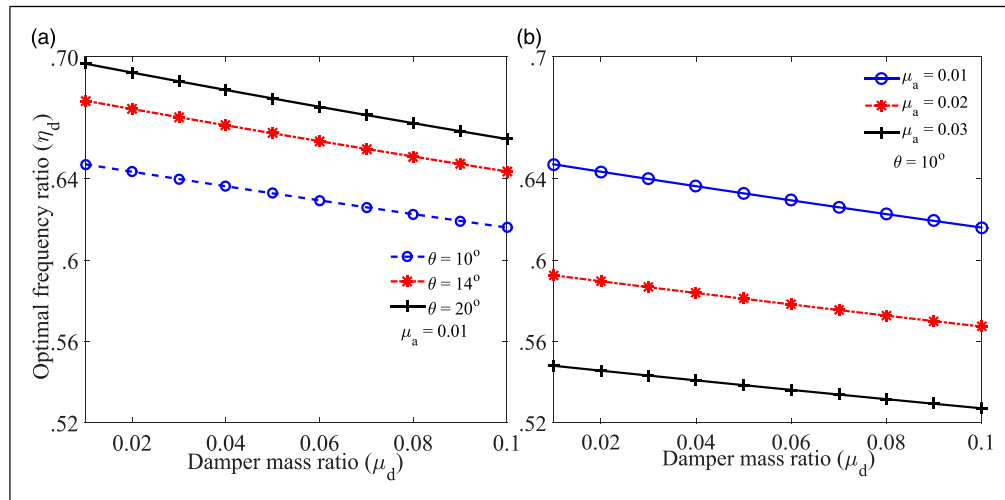


Figure 2. The variations of optimal frequency ratio of IAVTMD versus damper mass ratio for different values of (a) inertial angle and (b) amplifier's mass ratio.

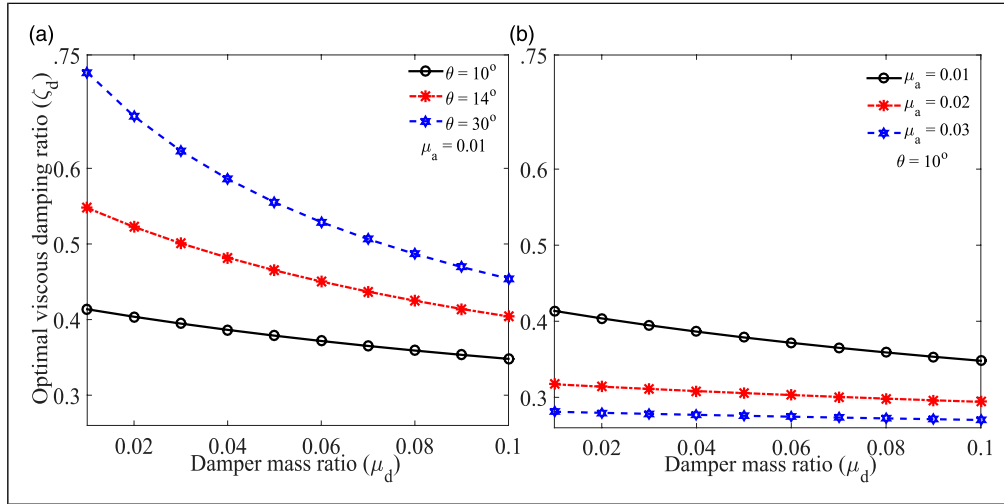


Figure 3. The variations of optimal viscous damping ratio of IAVTMD versus damper mass ratio for different values of (a) inertial angle and (b) amplifier's mass ratio.

H_∞ optimization for IAVTMD

The closed-form expressions for optimal design parameters of IAVTMD have also been derived through the H_∞ optimization method when the controlled structures are subjected to harmonic excitations. To perform that, the transfer function in equation (16) has been non-dimensionalized and expressed as

$$\begin{bmatrix} -\eta^2 + 2i\zeta_s\eta + 1 & \frac{-2i\eta\alpha\eta_d^3\mu_{dv}^2\zeta_d}{\alpha\eta_d^2\mu_{dv} + 2i\mu_{dv}\eta\eta_d\zeta_d} - \eta_d^2\mu_{dv} \\ -\mu_{dv}\eta^2 & -\mu_{dv}\eta^2 + \frac{2i\eta\alpha\eta_d^3\mu_{dv}^2\zeta_d}{\alpha\eta_d^2\mu_{dv} + 2i\mu_{dv}\eta\eta_d\zeta_d} + \eta_d^2\mu_{dv} \end{bmatrix} \begin{Bmatrix} X_s \\ X_d \end{Bmatrix} = - \begin{bmatrix} 1 \\ \mu_{dv} \end{bmatrix} \frac{A_g}{\omega_s^2} \quad (29)$$

The dynamic response of the primary structure has been derived as

$$H_s = \frac{X_s}{A_g\omega_s^2} = \frac{-2i(\mu_{dv} + 1)(\alpha + 1)\eta_d^2 + \eta^2}{\Delta} \eta\zeta_d \quad (30)$$

The dynamic response of IAVTMD has been derived as

$$H_d = \frac{X_d}{A_g\omega_s^2} = \frac{-4\eta^2\zeta_d\zeta_s + \alpha\eta_d + i2\eta(\alpha\zeta_s\eta_d + \zeta_d)}{\Delta} \quad (31)$$

Δ has been derived as

$$\begin{aligned} & 4\alpha\eta^2\zeta_d\zeta_s\eta_d^2 + \alpha\eta^2\mu_{dv}\eta_d^3 - \alpha\eta^4\omega_d + \alpha\eta^2\eta_d^3 \\ & - 4\eta^4\zeta_d\zeta_s + 4\eta^2\zeta_d\zeta_s\eta_d^2 + \alpha\eta^2\eta_d - \alpha\eta_d^3 \\ \Delta = & + i(2\alpha\eta^3\zeta_d\mu_{dv}\eta_d^2 + 2\alpha\eta^3\zeta_d\eta_d^2 + 2\eta^3\zeta_d\mu_{dv}\eta_d^2 \\ & + 2\alpha\eta^3\zeta_s\eta_d - 2\alpha\eta\zeta_s\eta_d^3 - 2\eta^5\zeta_d + 2\eta^3\zeta_d\eta_d^2 \\ & - 2\eta\alpha\eta_d^2\zeta_d + 2\eta^3\zeta_d - 2\eta\zeta_d\eta_d^2) \end{aligned} \quad (32)$$

The resultant of H_s has been summarized as

$$|H_s| = \sqrt{\frac{y_1^2 + \zeta_d^2 y_2^2}{y_3^2 + \zeta_d^2 y_4^2}} = \frac{y_2}{y_4} \sqrt{\frac{y_1^2 + \zeta_d^2}{y_2^2 + \zeta_d^2}} \quad (33)$$

From equation (33), the first restraint (Den Hartog, 1985) for H_∞ optimization has been derived as

$$\left| \frac{y_1}{y_2} \right| = \left| \frac{y_3}{y_4} \right| \quad (34)$$

An equation has been derived after applying equation (34) and expressed as

$$\begin{aligned}
& 2\eta^6 + (-2\alpha\mu_{dv}\eta_d^2 - 2\alpha\eta_d^2 - 4\mu_{dv}\eta_d^2 - 4\eta_d^2 - 2)\eta^4 \\
& + \left(\begin{aligned} & 2\alpha\mu_{dv}^2\eta_d^4 + 4\alpha\mu_{dv}\omega_d^4 + 2\mu_{dv}^2\eta_d^4 + 2\alpha\eta_d^4 \\ & + 4\mu_{dv}\eta_d^4 + \alpha\mu_{dv}\eta_d^2 + 2\eta_d^4 + 2\alpha\omega_d^2 + 2\mu_{dv}\eta_d^2 + 4\eta_d^2 \\ & - 2\alpha\mu_{dv}\eta_d^4 - 2\alpha\eta_d^4 - 2\mu_{dv}\eta_d^4 - 2\eta_d^4 \end{aligned} \right) \eta^2 = 0 \quad (35)
\end{aligned}$$

Equation (35) has been summarized as

$$\begin{aligned}
& \eta^6 + (-\eta_1^2 - \eta_2^2 - \eta_3^2)\eta^4 \\
& + (\eta_1^2\eta_2^2 + \eta_3^2\eta_1^2 + \eta_2^2\eta_3^2)\eta^2 - \eta_1^2\eta_2^2\eta_3^2 = 0 \quad (36)
\end{aligned}$$

Therefore, the roots for equation (35) have been derived as

$$\begin{aligned}
& \eta_1^2 + \eta_2^2 + \eta_3^2 = \alpha\mu_{dv}\eta_d^2 + \alpha\eta_d^2 + 2\mu_{dv}\eta_d^2 \\
& + 2\eta_d^2 + 1\eta_1^2\eta_2^2 + \eta_3^2\eta_1^2 + \eta_2^2\eta_3^2 = \alpha\mu_{dv}^2\eta_d^4 \\
& + 2\alpha\mu_{dv}\eta_d^4 + \mu_{dv}^2\eta_d^4 + \alpha\eta_d^4 + 2\mu_{dv}\eta_d^4 \quad (37) \\
& + 1/2\alpha\mu_{dv}\eta_d^2 + \eta_d^4 + \alpha\eta_d^2 + \mu_{dv}\eta_d^2 \\
& + 2\eta_d^2\eta_1^2\eta_2^2\eta_3^2 = \alpha\mu_{dv}\eta_d^4 + \alpha\eta_d^4 + \mu_{dv}\eta_d^4 + \eta_d^4
\end{aligned}$$

$$\begin{aligned}
& \left(\begin{aligned} & 2\alpha^2\mu_{dv}^3 + 6\alpha^2\mu_{dv}^2 + 6\alpha\mu_{dv}^3 + 6\alpha^2\mu_{dv} \\ & + 18\alpha\mu_{dv}^2 + 4\mu_{dv}^3 + 2\alpha^2 + 18\alpha\mu_{dv} \\ & + 12\mu_{dv}^2 + 6\alpha + 12\mu_{dv} + 4 \end{aligned} \right) \eta_d^4 \\
& + \left(\begin{aligned} & \alpha^2\mu_{dv}^2 + 3\alpha^2\mu_{dv} + 6\alpha\mu_{dv}^2 + 2\alpha^2 \\ & + 14\alpha\mu_{dv} + 6\mu_{dv}^2 + 8\alpha + 14\mu_{dv} + 8 \end{aligned} \right) \eta_d^2 \\
& + \alpha\mu_{dv} + 2\alpha + 2\mu_{dv} + 4
\end{aligned} = 0 \quad (43)$$

$$w_2\eta_d^4 + w_1\eta_d^2 + w_0 = 0 \quad (44)$$

$$\begin{aligned}
& (\eta_{d1})_{opt}^2 = \frac{-w_1 + \sqrt{w_1^2 - 4w_2w_0}}{2w_2} \quad \text{and} \\
& (\eta_{d2})_{opt}^2 = \frac{-w_1 - \sqrt{w_1^2 - 4w_2w_0}}{2w_2} \quad (45)
\end{aligned}$$

After applying equations (41) and (42), the closed-form expressions for $\eta_{1,2}^2$ are derived as

$$\eta_{1,2}^2 = \pm \sqrt{\frac{\alpha\mu_{dv}^2\eta_d^4 + 2\alpha\mu_{dv}\eta_d^4 + \mu_{dv}^2\eta_d^4 + \alpha\eta_d^4 + 2\mu_{dv}\eta_d^4}{+ 1/2\alpha\mu_{dv}\eta_d^2 + \eta_d^4 + \alpha\eta_d^2 + \mu_{dv}\eta_d^2 + 2\eta_d^2}} \quad (46)$$

From equation (33), the second constraint (Den Hartog, 1985) has been derived as

$$(H_s)_{\eta_1, \eta_2} = \left| \frac{y_2}{y_4} \right| \quad (38)$$

$$\eta_1^2 + \eta_2^2 = 0 \quad (39)$$

Equation (39) substitutes in the first equation of equation (37). Hence, η_3^2 derives as

$$\eta_3^2 = \alpha\mu_{dv}\eta_d^2 + \alpha\eta_d^2 + 2\mu_{dv}\eta_d^2 + 2\eta_d^2 + 1 \quad (40)$$

Equation (40) has been substitutes in the second and third equations of equation (37). Therefore, the closed-form expressions for $\eta_1^2\eta_2^2$ have been derived as

$$\begin{aligned}
& \eta_1^2\eta_2^2 = \alpha\mu_{dv}^2\eta_d^4 + 2\alpha\mu_{dv}\eta_d^4 + \mu_{dv}^2\eta_d^4 \\
& + \alpha\eta_d^4 + 2\mu_{dv}\eta_d^4 + 1/2\alpha\mu_{dv}\eta_d^2 \\
& + \eta_d^4 + \alpha\eta_d^2 + \mu_{dv}\eta_d^2 + 2\eta_d^2 \quad (41)
\end{aligned}$$

$$\eta_1^2\eta_2^2 = \frac{\eta_d^4(\mu_{dv} + 1)(\alpha + 1)}{1 + (\mu_{dv} + 1)(\alpha + 2)\eta_d^2} \quad (42)$$

Equations (41) and (42) are equated, and the closed-form expression for the optimal frequency ratio of IAVTMD has been derived as

$$\eta_{1,2}^2 = \pm \sqrt{\frac{\eta_d^4(\mu_{dv} + 1)(\alpha + 1)}{1 + (\mu_{dv} + 1)(\alpha + 2)\eta_d^2}} \quad (47)$$

The mathematical expressions for determining the closed-form expression for the optimal viscous damping ratio of IAVTMD have been derived as

$$\frac{\partial |H_s(\eta)|^2}{\partial \eta^2} \Big|_{\eta_{1,2}} = 0 \quad \text{and} \quad (\zeta_d)_{opt} = \sqrt{\frac{\zeta_{d1}^2 + \zeta_{d2}^2}{2}} \quad (48)$$

Therefore, the closed-form expression for the optimal viscous damping ratio of IAVTMD has been derived as

$$\begin{aligned}
& z_2\zeta_d^4 + z_1\zeta_d^2 + z_0 = 0 \quad \text{and} \quad \zeta_{d1, d2}^2 \\
& = \frac{-z_1 \pm \sqrt{-4z_2z_0 + z_1^2}}{2z_2} \quad (49)
\end{aligned}$$

The closed-form expressions for z_2 , z_1 , and z_0 have been derived as

$$\begin{aligned}
& -32\eta_{1,2}^4 \left((\alpha + 1)(\mu_{dv}\eta_{1,2}^2 + \eta_{1,2}^2 - 1)(\eta_{d1, d2})_{opt}^2 - \eta_{1,2}^4 + \eta_{1,2}^2 \right) \\
& \left((\alpha + 1)(\mu_{dv} + 1)(\eta_{d1, d2})_{opt}^2 - \eta_{1,2}^2 \right) \\
& \left((\alpha + 1)^2(\mu_{dv} + 1)^2\eta_{d1, d2}^4 + \eta_{1,2}^4 \right) \\
& \left(-2(\alpha + 1) \left((\eta_{1,2}^2 - 1/2)\mu_{dv} + \eta_{1,2}^2 \right) \eta_{d1, d2}^2 \right) \quad (50)
\end{aligned}$$

$$z_1 = -16 \eta_{d1,d2}^2 \eta_{1,2}^2 \alpha^2 \left(\begin{array}{l} (\alpha + 1)^2 (-1 + (\mu_{dv} + 1) \eta_{1,2}^2) (\mu_{dv} + 1)^3 \eta_{d1,d2}^8 \\ (\mu_{dv} + 1)^2 (\alpha + 2) \eta_{1,2}^4 \\ -2 \left(\begin{array}{l} -1/4 ((\alpha + 4) \mu_{dv} + 4 \alpha + 8) (\mu_{dv} + 1) \eta_{1,2}^2 \\ + \mu_{dv}/2 \\ (\alpha + 1) (\mu_{dv} + 1) \eta_{d1,d2}^6 \\ + \eta_{1,2}^2 ((\mu_{dv} + 1) \eta_{1,2}^2 - \mu_{dv}/2 - 1) \\ \left(\begin{array}{l} (\alpha^2 + 6 \alpha + 6) (\mu_{dv} + 1) \eta_{1,2}^2 \\ - 1/2 \mu_{dv} (\alpha^2 + 2 \alpha + 4) \end{array} \right) \eta_{d1,d2}^4 \\ -2 \left(\begin{array}{l} (\alpha + 2) (\mu_{dv} + 1) \eta_{1,2}^4 + \mu_{dv}/2 \\ + ((-3/4 \alpha - 2) \mu_{dv} - \alpha - 2) \eta_{1,2}^2 \end{array} \right) \eta_{1,2}^4 \eta_{d1,d2}^2 \\ + \eta_{1,2}^8 (\eta_{1,2}^2 - 1) \end{array} \right) \end{array} \right) \quad (51)$$

$$z_0 = -2 \left((\mu_{dv} + 1) \eta_{d1,d2}^2 - \eta_{1,2}^2 \right) \left((\mu_{dv} + 1) \eta_{1,2}^4 \right) \\ + \left((-2 \mu_{dv} - 2) \eta_{1,2}^2 + \mu_{dv} \right) \eta_{d1,d2}^2 + \eta_{1,2}^4 \\ \eta_{d1,d2}^4 \left((-1 + (\mu_{dv} + 1) \eta_{1,2}^2) \eta_{d1,d2}^2 - \eta_{1,2}^4 + \eta_{1,2}^2 \right) \alpha^4 \quad (52)$$

The variations of the optimal frequency ratio of IAVTMD versus damper mass ratio for the different values of inertial angles are shown in Figure 4(a). The system parameters are considered as $\mu_a = 0.01$ and $\alpha = 1.0$. The optimal frequency ratio of IAVTMD decreases as the inertial angle decreases.

The variations of the optimal frequency ratio of IAVTMD versus damper mass ratio for the different values of the amplifier's mass ratio are shown in Figure 4(b). The system parameters are considered as $\theta = 10^\circ$ and $\alpha = 1.0$. The optimal frequency ratio decreases as the damper mass ratio and amplifier's mass ratio increase. As a result, a higher damper mass ratio, a higher amplifier's mass ratio, and a lower inertial angle are recommended for H_∞ optimized IAVTMD for achieving a lower frequency ratio without reducing the static mass of the entire system. The variations of the optimal frequency ratio of IAVTMD versus damper mass ratio for the different values of inertial angles are shown in Figure 5(a). The system parameters are considered as $\mu_a = 0.01$ and $\alpha = 1.0$. The optimal frequency ratio of IAVTMD decreases as the inertial angle decreases.

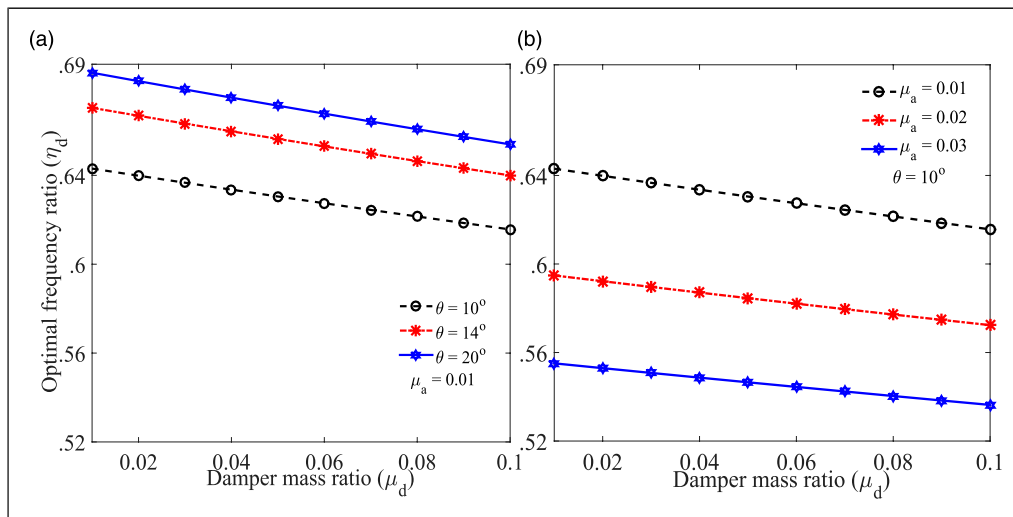


Figure 4. The variations of optimal frequency ratio of IAVTMD versus damper mass ratio for different values of (a) inertial angle and (b) amplifier's mass ratio.

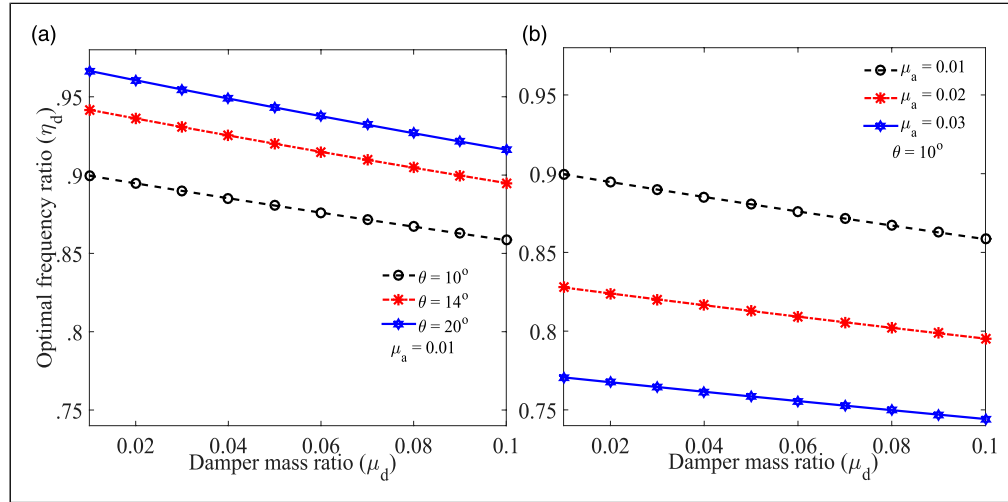


Figure 5. The variations of optimal frequency ratio of IAVTMD versus damper mass ratio for different values of (a) inertial angle and (b) amplifier's mass ratio.

The variations of the optimal frequency ratio of IAVTMD versus damper mass ratio for the different values of the amplifier's mass ratio are shown in Figure 5(b). The system parameters are considered as $\theta = 10^\circ$ and $\alpha = 1.0$. The optimal frequency ratio decreases as the damper mass ratio and amplifier's mass ratio increase. As a result, a higher damper mass ratio, a higher amplifier's mass ratio, and a lower inertial angle are recommended for H_∞ optimized IAVTMD for achieving a lower frequency ratio without reducing the static mass of the entire system. The variations of optimal viscous damping ratio of IAVTMD versus damper mass ratio for the different values of inertial angles are shown in Figure 6(a). The system parameters are considered as $\mu_a = 0.01$ and $\alpha = 1.0$. The optimal viscous damping ratio of IAVTMD decreases as the inertial angle decreases.

The variations of optimal viscous damping ratio of IAVTMD versus damper mass ratio for the different values of the amplifier's mass ratio are shown in Figure 6(b). The system parameters are considered as $\theta = 10^\circ$ and $\alpha = 1.0$. The optimal viscous damping ratio decreases as the damper mass ratio increases and decreases as the amplifier's mass ratio increases. As a result, a higher damper mass ratio, a moderate amplifier's mass ratio, and a lower inertial angle are recommended for H_∞ optimized IAVTMD to achieve an average viscous damping ratio without reducing the static mass of the entire controlled structure. The variations of optimal viscous damping ratio of IAVTMD versus damper mass ratio for the different values of inertial angles are shown in Figure 7(a). The system parameters are considered as $\mu_a = 0.01$ and $\alpha = 1.0$. The optimal viscous damping ratio of IAVTMD decreases as the inertial angle decreases.

The variations of the optimal viscous damping ratio of IAVTMD versus damper mass ratio for the different values of the amplifier's mass ratio are shown in Figure 7(b). The system parameters are considered as $\theta = 10^\circ$ and $\alpha = 1.0$. The optimal

viscous damping ratio decreases as the damper mass ratio increases and decreases as the amplifier's mass ratio increases. As a result, a higher damper mass ratio, a moderate amplifier's mass ratio, and a lower inertial angle are recommended for H_∞ optimized IAVTMD to achieve an average viscous damping ratio without reducing the static mass of the entire controlled structure.

Robustness of H_2 and H_∞ optimized IAVTMD

The variations of optimal displacements of primary structures controlled by H_2 optimized IAVTMD for different values of viscous damping ratio have been shown in Figure 8(a). The system parameters are considered as $\mu_d = 0.04$, $\mu_a = 0.01$, $\theta = 5^\circ$. The optimal frequency and viscous damping ratios are obtained as $\eta_d = 0.5058$ and $\zeta_d = 0.2619$. The dynamic responses are unrestrained at $\zeta_d = 0$, and the controlled structures vibrate at their Eigen frequencies, that is, $\eta = 0.4571, 1.107$. The anti-resonance point is located at $\eta = 0.6591$. The frequency regions are shifted from its Eigen frequency regions when ζ_d increases, that is, $\zeta_d > 0$. The maximum dynamic responses are minimized at their resonating frequency regions, that is, $\eta = 0.3804, 1.148$. The maximum peaks of dynamic responses are merged into one at $\zeta_d = \infty$. The frequency point is located at $\eta = 1.207$. An anti-resonance frequency point has also been located at $\eta = 0.5292$.

The variations of optimal displacements of primary structures controlled by H_∞ optimized IAVTMD for different values of viscous damping ratio have been shown in Figure 8(b). The system parameters are considered as $\mu_d = 0.04$, $\mu_a = 0.01$, $\theta = 5^\circ$. The optimal frequency and viscous damping ratios are obtained as $\eta_d = 0.5172$ and $\zeta_d = 0.3478$. The dynamic responses are unrestrained at $\zeta_d = 0$, and the controlled structures vibrate at their Eigen frequencies,

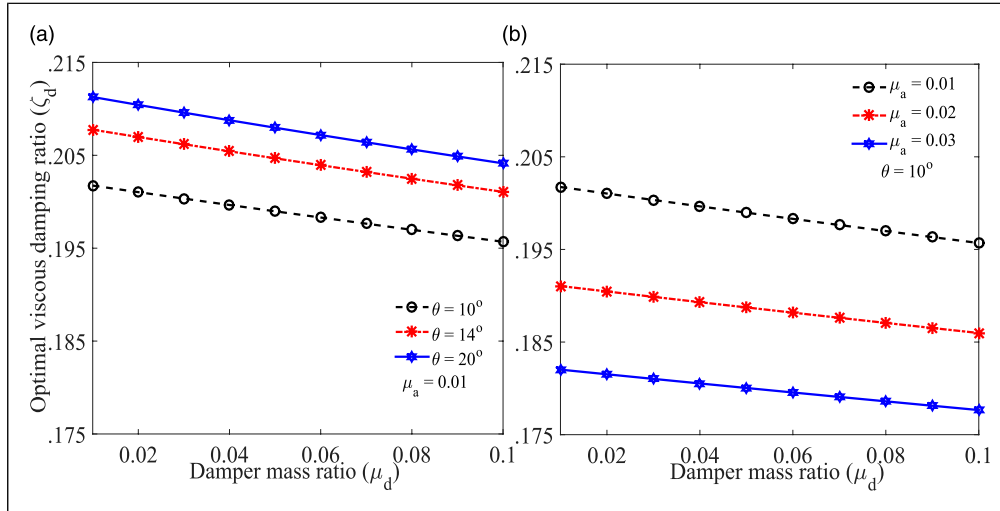


Figure 6. The variations of optimal viscous damping ratio of IAVTMD versus damper mass ratio for different values of (a) inertial angle and (b) amplifier's mass ratio.

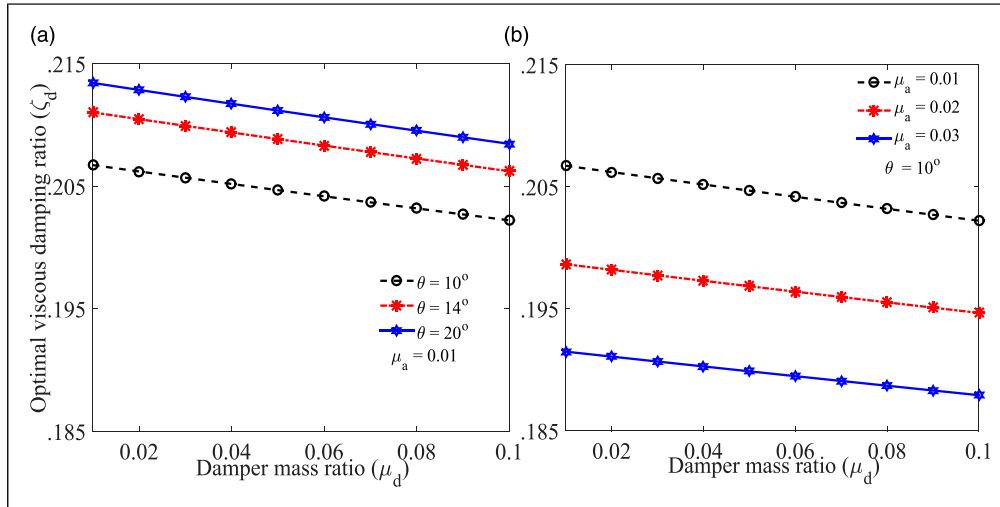


Figure 7. The variations of optimal viscous damping ratio of IAVTMD versus damper mass ratio for different values of (a) inertial angle and (b) amplifier's mass ratio.

that is, $\eta = 0.465, 1.113$. The anti-resonance point is located at $\eta = 0.6738$. The frequency regions are shifted from its Eigen frequency regions when ζ_d increases, that is, $\zeta_d > 0$. The maximum dynamic responses are minimized at their resonating frequency regions, that is, $\eta = 0.3488, 1.169$. The maximum peaks of dynamic responses are merged into one at $\zeta_d = \infty$. The frequency point is located at $\eta = 1.214$. An anti-resonance frequency point has also been located at $\eta = 0.5411$.

Comparison of dynamic responses

The dynamic responses of optimum IVATMD-controlled structures compared with

dynamic responses of structures controlled by optimum conventional tuned mass dampers

The variations of optimal dynamic responses of uncontrolled structures and structures controlled by H_2 optimized conventional TMD, inertial amplifier viscoelastic tuned mass damper have been displayed in Figure 9(a). The design parameters are listed in Table 1.

The closed-form expressions for optimal design parameters of H_2 optimized conventional tuned mass dampers (i.e., CTMD1, CTMD2) are accounted from CTMD1 (Warburton, 1982; Zilletti et al., 2012) and CTMD2 (Iwata, 1982). Equation (25) and (24) are applied to determine the optimal design parameters for H_2 optimized IAVTMD.

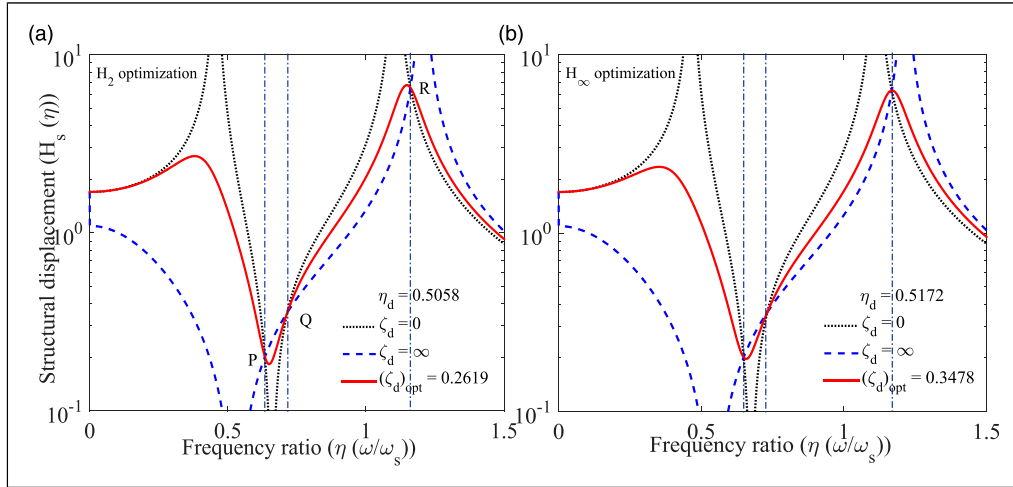


Figure 8. The variations of optimal displacements of primary structures controlled by (a) H_2 and (b) H_∞ optimized IAVTMD for different values of viscous damping ratio.

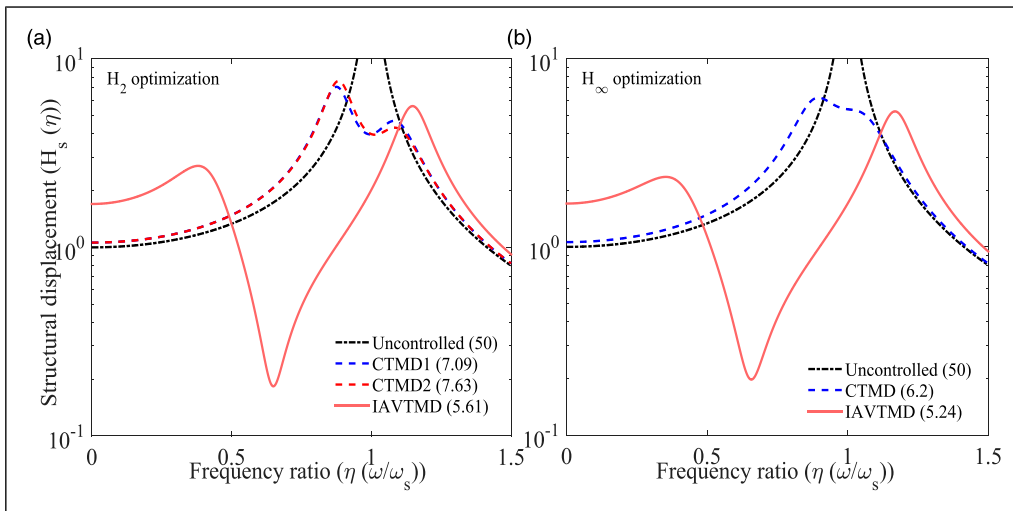


Figure 9. The variations of optimal displacements of primary structures controlled by (a) H_2 and (b) H_∞ optimized IAVTMD and conventional tuned mass dampers subjected to harmonic excitation.

Table 1. The optimal design parameters of H_2 optimized IAVTMD and conventional tuned mass dampers.

Symbols			H_2 optimization		
CTMD1	CTMD2	IVATMD	CTMD1	CTMD2	IVATMD
ζ_s	ζ_s	ζ_s	0.01	0.01	0.01
ζ_d	ζ_d	ζ_d	0.1198	0.1225	0.2619
η_d	η_d	η_d	0.9574	0.9713	0.5058
μ_d	μ_d	$\mu_d + 2\mu_a$	0.06	0.06	0.06
—	—	μ_d	0.06	0.06	0.04
—	—	μ_a	—	—	0.01
—	—	θ	—	—	5°

The maximum dynamic response of the uncontrolled structure has been obtained as 50. The maximum dynamic responses of the primary structures controlled by CTMD1, CTMD2, and IAVTMD have been obtained as 7.09, 7.63, and 5.61. The dynamic response capacity of H_2 optimized IAVTMD is significantly 20.87% and 26.47% superior to the dynamic response capacity of H_2 optimized conventional TMD, respectively. The variations of optimal dynamic responses of uncontrolled structures and structures controlled by H_∞ optimized conventional tuned mass damper, inertial amplifier viscoelastic tuned mass damper have been displayed in Figure 9(b). The design parameters are listed in Table 2. The closed-form expressions for optimal design parameters of H_∞ optimized conventional tuned mass damper (i.e., CTMD) are accounted from conventional tuned mass damper's (CTMD) (Den Hartog and Ormondroyd, 1928; Krenk, 2005; Nishihara and Asami, 2002). Equations (45) and (49) are applied to determine the optimal design parameters for H_∞ optimized IAVTMD. The maximum dynamic response of the uncontrolled structure has been obtained as 50. The maximum

dynamic responses of the primary structures controlled by H_∞ optimized CTMD and IAVTMD have been obtained as 6.2 and 5.24. The dynamic response capacity of H_∞ optimized IAVTMD is significantly 15.48% superior to the dynamic response capacity of H_∞ optimized conventional tuned mass damper. The dynamic response capacities of H_2 and H_∞ optimized conventional TMD and inertial amplifier TMD are also evaluated when the controlled structures are subjected to random white-noise excitations. Therefore, the variations of optimal dynamic responses of uncontrolled structures and structures controlled by H_2 optimized conventional TMD, inertial amplifier viscoelastic tuned mass damper subjected to random-white noise excitations have been displayed in Figure 10(a). The design parameters are listed in Table 1.

The closed-form expressions for optimal design parameters of H_2 optimized conventional tuned mass dampers (i.e., CTMD1, CTMD2) are accounted from CTMD1 (Warburton, 1982, Zilletti et al., 2012) and CTMD2 (Iwata, 1982). Equations (24) and (25) are applied to determine the optimal design parameters for H_2 optimized IAVTMD. The maximum dynamic response of the uncontrolled structure has been obtained as 3.3023×10^7 dB/Hz. The maximum dynamic responses of the primary structures controlled by CTMD1, CTMD2, and IAVTMD have been obtained as 6.8883×10^5 dB/Hz, 8.7366×10^5 dB/Hz, and 4.5478×10^5 dB/Hz. The dynamic response capacity of H_2 optimized IAVTMD is significantly 33.97% and 47.94% superior to the dynamic response capacity of H_2 optimized conventional TMD, respectively.

The variations of optimal dynamic responses of uncontrolled structures and structures controlled by H_∞ optimized conventional tuned mass damper, inertial amplifier viscoelastic tuned mass damper subjected to random-white noise excitations have been displayed in Figure 10(b). The design parameters are listed in Table 2. The closed-form expressions for optimal design parameters of H_∞ optimized

Table 2. The optimal design parameters of H_∞ optimized IAVTMD and conventional tuned mass dampers.

Symbols		H_∞ optimization	
CTMD	IVATMD	CTMD	IVATMD
ζ_s	ζ_s	0.01	0.01
ζ_d	ζ_d	0.1682	0.3478
η_d	η_d	0.9434	0.5172
μ_d	$\mu_d + 2\mu_a$	0.06	0.06
μ_d	μ_d	0.06	0.04
—	μ_a	—	0.01
—	θ	—	5°

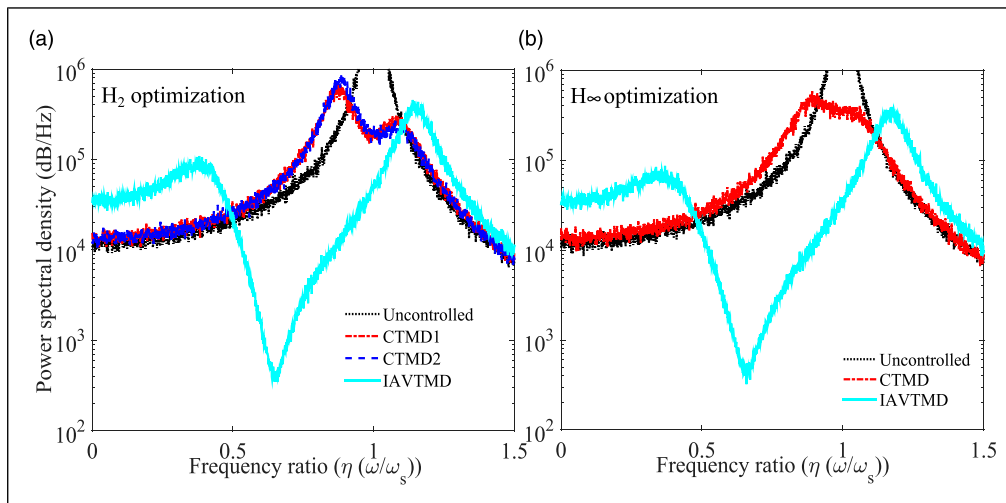


Figure 10. The variations of optimal displacements of primary structures controlled by (a) H_2 and (b) H_∞ optimized IAVTMD and conventional tuned mass dampers subjected to random-white noise excitation.

conventional tuned mass damper (i.e., CTMD) are accounted from CTMD (Den Hartog and Ormondroyd, 1928; Krenk, 2005; Nishihara and Asami, 2002). Equations (45) and (49) are applied to determine the optimal design parameters for H_∞ optimized IAVTMD. The maximum dynamic response of the uncontrolled structure has been obtained as 3.6872×10^7 dB/Hz. The maximum dynamic responses of the primary structures controlled by H_∞ optimized CTMD and IAVTMD have been obtained as 5.8581×10^5 dB/Hz and 3.9023×10^5 dB/Hz. The dynamic response capacity of H_∞ optimized IAVTMD is significantly 33.38% superior to the dynamic response capacity of H_∞ optimized conventional tuned mass damper.

The comparison of vibration reduction capacity of optimum IVATMD to the optimum tuned mass damper inerters

The equations of motion of a single degree of freedom system controlled by tuned mass damper inerters (TMDI) are derived using Newton's second law and expressed as

$$\begin{aligned} (m_d + m_b)\ddot{x}_d + c_d(\dot{x}_d - \dot{x}_s) + k_d(x_d - x_s) &= -m_d\ddot{x}_g \\ m_s\ddot{x}_s - c_d\dot{x}_d + (c_s + c_d)\dot{x}_d - k_d x_d + (k_s + k_d)x_d &= -m_s\ddot{x}_g \end{aligned} \quad (53)$$

The steady-state solutions for harmonic excitation are applied to equation (53), and the transfer function derives as

$$\begin{bmatrix} (\mu_d + \beta)q^2 + 2\mu_d\omega_d\zeta_d q + \mu_d\omega_d^2 & -2\mu_d\omega_d\zeta_d q - \mu_d\omega_d^2 \\ -2\mu_d\omega_d\zeta_d q - \mu_d\omega_d^2 & q^2 + q(2\mu_d\omega_d\zeta_d + 2\zeta_s\omega_s) + \omega_s^2 + \mu_d\omega_d^2 \end{bmatrix} \begin{Bmatrix} X_d \\ X_s \end{Bmatrix} = - \begin{bmatrix} \mu_d \\ 1 \end{bmatrix} A_g \quad (54)$$

where $q = i\omega$, $x_s = X_s e^{i\omega t}$, $x_d = X_d e^{i\omega t}$, and $\ddot{x}_g = A_g e^{i\omega t}$. The damper mass ratio: $\mu_d = m_d/m_s$, inerter mass ratio: $\beta = m_b/m_s$. The dynamic responses of TMDI and primary structure derive as

$$\sigma_{x_s}^2 = \frac{S_{0\pi} \begin{pmatrix} 4\beta\zeta_d^2\mu_d^4\omega_d^2\omega_s^2 + 4\zeta_d^2\mu_d^5\omega_d^2\omega_s^2 + \beta^2\mu_d^4\omega_d^4 + 8\beta\zeta_d^2\mu_d^3\omega_d^2\omega_s^2 \\ + 2\beta\mu_d^5\omega_d^4 + 12\zeta_d^2\mu_d^4\omega_d^2\omega_s^2 + \mu_d^6\omega_d^4 + 2\beta^2\mu_d^3\omega_d^4 + \beta^2\mu_d^3\omega_d^2\omega_s^2 \\ + 4\beta\zeta_d^2\mu_d^2\omega_d^2\omega_s^2 + 6\beta\mu_d^4\omega_d^4 + 2\beta\mu_d^4\omega_d^2\omega_s^2 + 12\zeta_d^2\mu_d^3\omega_d^2\omega_s^2 \\ + 4\mu_d^5\omega_d^4 + \mu_d^5\omega_d^2\omega_s^2 + \beta^2\mu_d^2\omega_d^4 + 6\beta\mu_d^3\omega_d^4 + 4\zeta_d^2\mu_d^2\omega_d^2\omega_s^2 \\ + 6\mu_d^4\omega_d^4 - \beta^2\mu_d\omega_d^2\omega_s^2 + 2\beta\mu_d^2\omega_d^4 - 4\beta\mu_d^2\omega_d^2\omega_s^2 + 4\mu_d^3\omega_d^4 \\ - 3\mu_d^3\omega_d^2\omega_s^2 + \beta^2\omega_s^4 - 2\beta\mu_d\omega_d^2\omega_s^2 + 2\beta\mu_d\omega_s^4 + \mu_d^2\omega_d^4 \\ - 2\mu_d^2\omega_d^2\omega_s^2 + \mu_d^2\omega_s^4 \\ 2\zeta_d\mu_d\omega_d\omega_s^6(\mu_d + \beta)^2 \end{pmatrix}}{2\zeta_d\mu_d\omega_d\omega_s^6(\mu_d + \beta)^2} \quad (58)$$

$$H_d = \frac{X_d}{A_g} = \frac{- (2\mu_d\omega_d\zeta_d q + 2q\zeta_d\omega_d + 2q\zeta_s\omega_s + \mu_d\omega_d^2 + q^2 + \omega_d^2 + \omega_s^2)\mu_d}{\Delta} \quad (55)$$

$$H_s = \frac{X_s}{A_g} = \frac{- 2\mu_d^2\omega_d\zeta_d q - 2\mu_d\omega_d\zeta_d q - \omega_d^2\mu_d^2 - q^2\beta - q^2\mu_d - \mu_d\omega_d^2}{\Delta} \quad (56)$$

$$\begin{aligned} \Delta = & (\mu_d + \beta)q^4 + (2\beta\zeta_d\mu_d\omega_d + 2\zeta_d\omega_d\mu_d^2 + 2\beta\zeta_s\omega_s \\ & + 2\mu_d\omega_d\zeta_d + 2\zeta_s\mu_d\omega_s)q^3 + (4\zeta_d\zeta_s\mu_d\omega_d\omega_s + \beta\mu_d\omega_d^2 \\ & + \omega_d^2\mu_d^2 + \beta\omega_s^2 + \mu_d\omega_d^2 + \mu_d\omega_s^2)q^2 \\ & + (2\zeta_d\mu_d\omega_d\omega_s^2 + 2\zeta_s\mu_d\omega_d^2\omega_s)q + \mu_d\omega_d^2\omega_s^2 \end{aligned} \quad (57)$$

H_2 and H_∞ optimization methods are applied to derive optimal closed-form solutions for TMDI subjected to harmonic and random excitations.

H_2 optimization

The standard deviation of equation (56) derives using equation (20) and expressed as

The exact closed-form expression for the damping ratio of TMDI derives using equation (58), the first equation of equation (23) and expressed as

$$\zeta_d = \sqrt{\frac{\begin{aligned} &\beta^2 \mu_d^4 \omega_d^4 + 2\beta \mu_d^5 \omega_d^4 + \mu_d^6 \omega_d^4 + 2\beta^2 \mu_d^3 \omega_d^4 + \beta^2 \mu_d^3 \omega_d^2 \omega_s^2 \\ &+ 6\beta \mu_d^4 \omega_d^4 + 2\beta \mu_d^4 \omega_d^2 \omega_s^2 + 4\mu_d^5 \omega_d^4 + \mu_d^5 \omega_d^2 \omega_s^2 + \beta^2 \mu_d^2 \omega_d^4 \\ &+ 6\beta \mu_d^3 \omega_d^4 + 6\mu_d^4 \omega_d^4 - \beta^2 \mu_d \omega_d^2 \omega_s^2 + 2\beta \mu_d^2 \omega_d^4 - 4\beta \mu_d^2 \omega_d^2 \omega_s^2 \\ &+ 4\mu_d^3 \omega_d^4 - 3\mu_d^3 \omega_d^2 \omega_s^2 + \beta^2 \omega_s^4 - 2\beta \mu_d \omega_d^2 \omega_s^2 + 2\beta \mu_d \omega_s^4 \\ &+ \mu_d^2 \omega_d^4 - 2\mu_d^2 \omega_d^2 \omega_s^2 + \mu_d^2 \omega_s^4 \end{aligned}}{4\beta \mu_d^4 \omega_d^2 \omega_s^2 + 4\mu_d^5 \omega_d^2 \omega_s^2 + 8\beta \mu_d^3 \omega_d^2 \omega_s^2 + 12\mu_d^4 \omega_d^2 \omega_s^2 \\ + 4\beta \mu_d^2 \omega_d^2 \omega_s^2 + 12\mu_d^3 \omega_d^2 \omega_s^2 + 4\mu_d^2 \omega_d^2 \omega_s^2}} \quad (59)$$

The optimal closed-form solution for the natural frequency of TMDI derives using the modified version of equation (58), second equation of equation (23) and expressed as (Chowdhury and Banerjee, 2022b)

$$(\omega_d)_{opt} = \frac{\omega_s \sqrt{2\mu_d(\mu_d + 1)(\beta^2 + 2\beta\mu_d + \mu_d^2 + 2\beta + 2\mu_d - \beta^2\mu_d - 2\beta\mu_d^2 - \mu_d^3)}}{2\mu_d(\mu_d + 1)(\beta + \mu_d + 1)} \quad (60)$$

of inerter mass ratio have been displayed in Figure 11(b). The optimal damping ratio increases as the damper mass ratio increases; in contrast, it increases as the inerter mass ratio increases. Accordingly, a higher damper mass ratio and a lower inerter mass ratio are recommended to produce H_2 -optimized TMDI with a lower frequency and damping ratio in an affordable range.

H_∞ optimization

Equation (54) rewritten in non-dimensional form to apply H_∞ optimization method and expressed as

$$\begin{bmatrix} -(\mu_d + \beta)\eta^2 + 2i\mu_d\eta_d\zeta_d\eta + \mu_d\eta_d^2 & -2i\mu_d\eta_d\zeta_d\eta - \mu_d\eta_d^2 \\ -2i\mu_d\eta_d\zeta_d\eta - \mu_d\eta_d^2 & 2i\mu_d\eta_d\zeta_d\eta + 2i\eta\zeta_s + \mu_d\eta_d^2 - \eta^2 + 1 \end{bmatrix} \begin{Bmatrix} X_d \\ X_s \end{Bmatrix} = - \begin{bmatrix} \mu_d \\ 1 \end{bmatrix} \frac{A_g}{\omega_s^2} \quad (62)$$

Equation (60) substitutes in equation (59) and the optimal closed-form solution for the damping ratio of TMDI derives as (Chowdhury et al., 2023a)

$$(\zeta_d)_{opt} = \frac{\sqrt{2}}{4} \sqrt{\frac{(\mu_d^2 + (\beta - 3)\mu_d - 3\beta - 4)(\mu_d + \beta)^2}{(\beta + \mu_d + 1)\mu_d(\mu_d^2 + (\beta - 1)\mu_d - \beta - 2)}} \quad (61)$$

The variations of optimal frequency ratio of H_2 -optimized TMDI versus damper mass ratio for different values of inerter mass ratio have been shown in Figure 11(a). The optimal frequency ratio decreases as the damper mass ratio increases; in contrast, it increases as the inerter mass ratio increases.

The differences in optimal damping ratio of H_2 -optimized TMDI versus damper mass ratio for different values

where $\eta = \omega/\omega_s$ and TMDI's frequency ratio: $\eta_d = \omega_d/\omega_s$. The dynamic responses of TMDI and primary structure derive as

$$H_d = \frac{X_d}{A_g} \omega_s^2 = \frac{\eta_d^2 \mu_d^2 - \eta^2 \mu_d + \mu_d \eta_d^2 + \mu_d + i(2\mu_d^2 \eta_d \zeta_d \eta + 2\mu_d \eta_d \zeta_d \eta + 2\mu_d \eta \zeta_s)}{\Delta} \quad (63)$$

$$H_s = \frac{X_s}{A_g} \omega_s^2 = \frac{\eta_d^2 \mu_d^2 - \eta^2 \beta - \eta^2 \mu_d + \mu_d \eta_d^2 + i(2\mu_d^2 \eta_d \zeta_d \eta + 2\mu_d \eta_d \zeta_d \eta)}{\Delta} \quad (64)$$

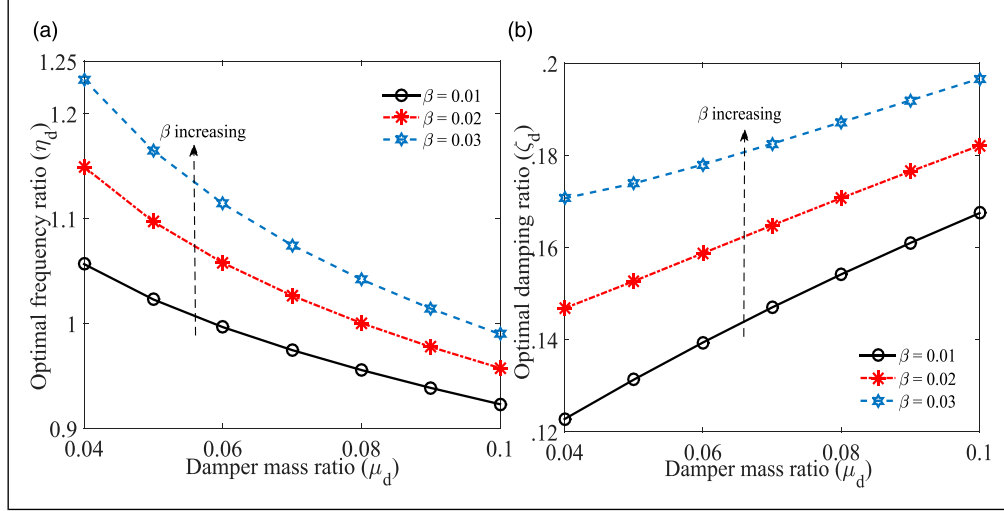


Figure 11. The variations of optimal (a) frequency and (b) damping ratio of H_2 -optimized TMDI versus damper mass ratio for different values of inerter mass ratio.

$$\begin{aligned} \Delta = & \beta \eta_d^2 \mu_d + 4 \eta_d^2 \zeta_d \zeta_s \eta_d \mu_d \\ & + \eta_d^2 \mu_d^2 - \beta \eta_d^4 - \eta_d^4 \mu_d + \eta_d^2 \mu_d + \eta_d^2 \beta + \eta_d^2 \mu_d \\ & - \mu_d \eta_d^2 + i(2\beta \eta_d^3 \zeta_d \eta_d \mu_d + 2 \eta_d^3 \zeta_d \eta_d \mu_d^2 + 2 \\ & \eta_d^3 \zeta_d \eta_d \mu_d + 2\beta \eta_d^3 \zeta_s + 2 \eta_d^3 \zeta_s \mu_d - 2 \\ & \eta_d \zeta_s \eta_d^2 \mu_d - 2 \mu_d \eta_d \zeta_d \eta_d) \end{aligned} \quad (65)$$

Equation (64) rewrites in the form of equation (33), in addition, equation (34) applies to derive closed-form solution for $\eta_1^2 + \eta_2^2$ and expressed as

$$\begin{aligned} & (\beta^2 + 3\beta\mu_d + 2\mu_d^2 + 2\beta + 2\mu_d)\eta^4 \\ & + \left(\begin{aligned} -2\beta\eta_d^2\mu_d^2 - 2\eta_d^2\mu_d^3 - 2\beta\eta_d^2\mu_d - 4\eta_d^2\mu_d^2 \\ -2\eta_d^2\mu_d - \beta\mu_d - \mu_d^2 - 2\beta - 2\mu_d \end{aligned} \right) \eta^2 = 0 \\ & + 2\eta_d^2\mu_d^2 + 2\eta_d^2\mu_d \\ & \eta_1^2 + \eta_2^2 = \frac{2\eta_d^2\mu_d^3 + (2\beta\eta_d^2 + 4\eta_d^2 + 1)\mu_d^2 + (2\beta\eta_d^2 + 2\eta_d^2 + \beta + 2)\mu_d + 2\beta}{(\beta + 2\mu_d + 2)(\beta + \mu_d)} \end{aligned} \quad (66)$$

$$\eta_1^2 \eta_2^2 = \frac{2\mu_d \eta_d^2 (\mu_d + 1)}{(\beta + 2\mu_d + 2)(\beta + \mu_d)}$$

The second constraint of equation (33) in the form of equation (38) applies and $\eta_1^2 + \eta_2^2$ derives as

$$\eta_1^2 + \eta_2^2 = \frac{2}{(\beta + \mu_d + 1)} \quad (67)$$

Equating second equation of equations (66) and (67), the exact closed-form expression for optimal frequency ratio derives as

$$\begin{aligned} & (2\beta^2\mu_d^2 + 4\beta\mu_d^3 + 2\mu_d^4 + 2\beta^2\mu_d + 8\beta\mu_d^2 \\ & + 6\mu_d^3 + 4\beta\mu_d + 6\mu_d^2 + 2\mu_d)\eta_d^2 \\ & + \beta^2\mu_d + 2\beta\mu_d^2 + \mu_d^3 - \beta\mu_d - \mu_d^2 - 2\beta - 2\mu_d = 0 \\ & (\eta_d)_{opt} = \sqrt{\frac{6\beta\mu_d^2 + 6\mu_d^3 + 4\beta\mu_d + 4\mu_d^2 - 2\beta^2\mu_d^3 - 4\beta\mu_d^4 - 2\mu_d^5 - 2\beta^2\mu_d^2 - 2\beta\mu_d^3}{2\mu_d(\mu_d + 1)(\beta + \mu_d + 1)}} \end{aligned} \quad (68)$$

Using, equations (66)–(68), the optimal closed-form solutions for each root η_1^2 and η_2^2 derives as

$$(\eta_{1,2}^2)_{opt} = \frac{\beta + 2\mu_d + 2 + \sqrt{\beta^2\mu_d + 3\beta\mu_d^2 + 2\mu_d^3 + \beta^2 + 5\beta\mu_d + 4\mu_d^2 + 2\beta + 2\mu_d}}{(\beta + 2\mu_d + 2)(\beta + \mu_d + 1)} \quad (69)$$

Accordingly, the exact closed-form expression for optimal damping ratio derives using equation (48) and is expressed as

$$A_0\zeta_d^4 + B_0\zeta_d^2 + C_0 = 0 \text{ and } \zeta_{d1,d2}^2 = \frac{-B_0 \pm \sqrt{B_0^2 - 4A_0C_0}}{2A_0} \quad (70)$$

where A_0 , B_0 , and C_0 are derived as

$$A_0 = -32 \mu_d^4 \eta_{1,2}^4 (\beta + \mu_d + 1) (\mu_d + 1)^2 (-1 + (\beta + \mu_d + 1) \eta_{1,2}^2) \eta_d^4 \quad (71)$$

$$B_0 = (-4(\beta + \mu_d)^2 \eta_d^2 \mu_d^2 (4\mu_d^2 + (2\beta + 8)\mu_d + \beta^2 + 2\beta + 4)) \eta_{1,2}^8 + \left(\begin{array}{l} 16(\beta + \mu_d)(\mu_d + 1) \eta_d^2 \mu_d^2 \\ (2\mu_d^3 \eta_d^2 + (1 + (3\beta + 4)\eta_d^2) \mu_d^2) \\ + (\beta + 1)(1 + (\beta + 2)\eta_d^2) \mu_d + \beta \end{array} \right) \eta_{1,2}^6 + B_{03} \eta_{1,2}^4 + 16 \eta_d^6 \mu_d^4 (\mu_d + 1)^2 (\beta + \mu_d + 1) \eta_{1,2}^2 \quad (72)$$

$$B_{03} = -16 \beta^2 \eta_d^6 \mu_d^6 - 32 \beta \eta_d^6 \mu_d^7 - 16 \eta_d^6 \mu_d^8 - 32 \beta^2 \eta_d^6 \mu_d^5 - 96 \beta \eta_d^6 \mu_d^6 - 64 \eta_d^6 \mu_d^7 - 16 \beta^2 \eta_d^6 \mu_d^4 - 96 \beta \eta_d^6 \mu_d^5 - 96 \eta_d^6 \mu_d^6 - 8 \beta^2 \eta_d^4 \mu_d^5 - 32 \beta \eta_d^6 \mu_d^4 - 16 \beta \eta_d^4 \mu_d^6 - 64 \eta_d^6 \mu_d^5 - 8 \eta_d^4 \mu_d^7 - 32 \beta^2 \eta_d^4 \mu_d^4 - 80 \beta \eta_d^4 \mu_d^5 - 16 \eta_d^6 \mu_d^4 - 48 \eta_d^4 \mu_d^6 - 24 \beta^2 \eta_d^4 \mu_d^3 - 96 \beta \eta_d^4 \mu_d^4 - 72 \eta_d^4 \mu_d^5 - 4 \beta^2 \eta_d^2 \mu_d^4 - 32 \beta \eta_d^4 \mu_d^3 - 8 \beta \eta_d^2 \mu_d^5 - 32 \eta_d^4 \mu_d^4 - 4 \eta_d^2 \mu_d^6 - 8 \beta^2 \eta_d^2 \mu_d^3 - 16 \beta \eta_d^2 \mu_d^4 - 8 \eta_d^2 \mu_d^5 \quad (73)$$

$$C_0 = (-2\beta^4 - 8\beta^3\mu_d - 12\beta^2\mu_d^2 - 8\beta\mu_d^3 - 2\mu_d^4) \eta_{1,2}^{10} + 2(4\eta_d^2\mu_d^2 + (1 + (\beta + 4)\eta_d^2)\mu_d + \beta) \eta_{1,2}^8 (\beta + \mu_d)^3 - 8\eta_{1,2}^6 (3/2\eta_d^2\mu_d^2 + (1 + (\beta + 3/2)\eta_d^2)\mu_d + \beta) (\mu_d + 1) \eta_d^2 (\beta + \mu_d)^2 \mu_d + C_{03} \eta_{1,2}^4 + C_{02} \eta_{1,2}^2 + 2\eta_d^6 ((\mu_d + 1)(\mu_d + \beta + 1) \eta_d^2 + \beta + \mu_d) \mu_d^4 (\mu_d + 1) \quad (74)$$

$$C_{03} = 2\beta^3 \eta_d^6 \mu_d^4 + 12\beta^2 \eta_d^6 \mu_d^5 + 18\beta \eta_d^6 \mu_d^6 + 8\eta_d^6 \mu_d^7 + 2\beta^3 \eta_d^6 \mu_d^3 + 22\beta^2 \eta_d^6 \mu_d^4 + 44\beta \eta_d^6 \mu_d^5 + 24\eta_d^6 \mu_d^6 + 10\beta^2 \eta_d^6 \mu_d^3 + 34\beta \eta_d^6 \mu_d^4 + 24\eta_d^6 \mu_d^5 + 10\eta_d^4 \mu_d^6 + 4\beta^3 \eta_d^4 \mu_d^3 + 18\beta^2 \eta_d^4 \mu_d^4 + 8\beta \eta_d^6 \mu_d^3 + 24\beta \eta_d^4 \mu_d^5 + 8\eta_d^6 \mu_d^4 + 2\beta^3 \eta_d^4 \mu_d^2 + 26\beta^2 \eta_d^4 \mu_d^3 + 46\beta \eta_d^4 \mu_d^4 + 22\eta_d^4 \mu_d^5 + 12\beta^2 \eta_d^4 \mu_d^2 + 24\beta \eta_d^4 \mu_d^3 + 2\eta_d^2 \mu_d^5 + 12\eta_d^4 \mu_d^4 + 2\beta^3 \eta_d^2 \mu_d^2 + 6\beta^2 \eta_d^2 \mu_d^3 + 6\beta \eta_d^2 \mu_d^4 \quad (75)$$

$$C_{02} = -2\beta^2 \eta_d^8 \mu_d^6 - 4\beta \eta_d^8 \mu_d^7 - 2\eta_d^8 \mu_d^8 - 4\beta^2 \eta_d^8 \mu_d^5 - 12\beta \eta_d^8 \mu_d^6 - 8\eta_d^8 \mu_d^7 - 2\beta^2 \eta_d^8 \mu_d^4 - 12\beta \eta_d^8 \mu_d^5 - 12\eta_d^8 \mu_d^6 - 4\beta^2 \eta_d^6 \mu_d^5 - 4\beta \eta_d^8 \mu_d^4 - 8\beta \eta_d^6 \mu_d^6 - 8\eta_d^8 \mu_d^5 - 4\eta_d^6 \mu_d^7 - 8\beta^2 \eta_d^6 \mu_d^4 - 24\beta \eta_d^6 \mu_d^5 - 2\eta_d^8 \mu_d^4 - 16\eta_d^6 \mu_d^6 - 4\beta^2 \eta_d^6 \mu_d^3 - 24\beta \eta_d^6 \mu_d^4 - 20\eta_d^6 \mu_d^5 - 2\beta^2 \eta_d^4 \mu_d^4 - 8\beta \eta_d^6 \mu_d^3 - 4\beta \eta_d^4 \mu_d^5 - 8\eta_d^6 \mu_d^4 - 2\eta_d^4 \mu_d^6 - 4\beta^2 \eta_d^4 \mu_d^3 - 8\beta \eta_d^4 \mu_d^4 - 4\eta_d^4 \mu_d^5 \quad (76)$$

The variations of optimal frequency ratio of H_∞ -optimized TMDI versus damper mass ratio for different values of inerter mass ratio have been shown in Figure 12(a).

The optimal frequency ratio decreases as the damper mass ratio increases; in contrast, it increases as the inerter mass ratio increases. The differences in optimal damping ratio of H_∞ -optimized TMDI versus damper mass ratio for different values of inerter mass ratio have been displayed in Figure 12(b). The optimal damping ratio increases as the damper mass ratio increases; in contrast, it increases as the inerter mass ratio increases. Accordingly, a higher damper mass ratio and a lower inerter mass ratio are recommended to produce H_∞ -optimized TMDI with a lower frequency and damping ratio in an affordable range.

Robustness of H_2 and H_∞ optimized TMDI

The variations of optimal dynamic responses of structures controlled by H_2 optimized TMDI versus frequency ratio for different values of damping ratio have been shown in Figure 13(a).

The H_2 optimized TMDI's design parameters are listed in Table 3 and $\zeta_s = 0$. Overall, the detailed values of optimal design parameters of H_2 and H_∞ optimized TMDI, IAVTMD are listed in Table 3.

At $\zeta_d = 0$, the controlled dynamic systems oscillate to their eigen frequencies, that is, $\eta = 0.8546$ and $\eta = 1.093$. The frequency points are shifted from these eigen frequencies at $\zeta_d > 0$. At $(\zeta_d)_{opt} = 0.1313$, the resonance occurs, and the maximum displacement of the primary structure minimizes effectively. The resonating frequencies are obtained at $\eta = 0.8656$ and $\eta = 1.07$. After increasing $\zeta_d > (\zeta_d)_{opt}$, the dynamic responses are slightly increases and massively increases at $\zeta_d = \infty$. One

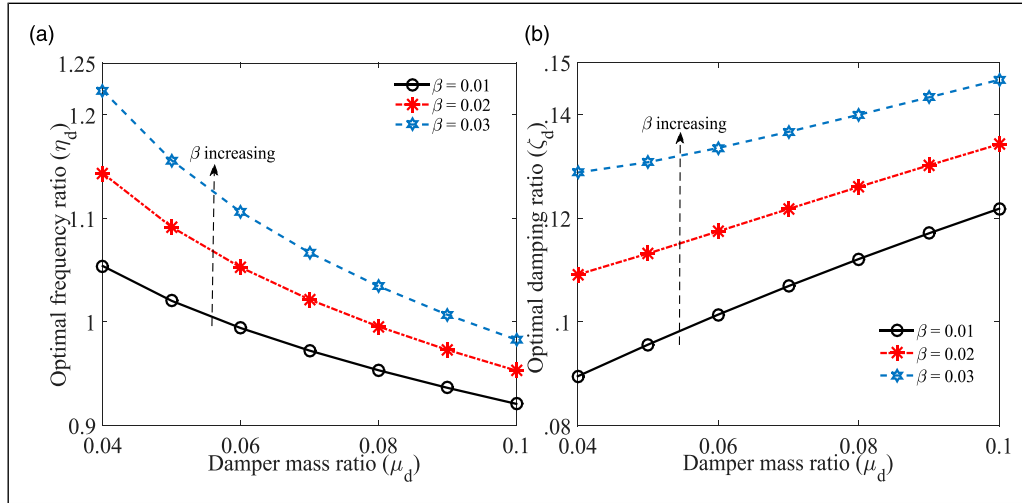


Figure 12. The variations of optimal (a) frequency and (b) damping ratio of H_∞ -optimized TMDI versus damper mass ratio for different values of inerter mass ratio.

frequency point locates at $\eta = 0.9713$. The maximum optimal dynamic response of H_2 optimized TMDI-controlled primary structure determines as 6.4512. The variations of optimal dynamic responses of structures controlled by H_∞ optimized TMDI versus frequency ratio for different values of damping ratio have been shown in Figure 13(b). The H_∞ optimized TMDI's design parameters are listed in Table 3 and $\zeta_s = 0$. $\eta = 0.8532$ and $\eta = 1.091$ are the eigen frequencies at undamped condition, that is, $\zeta_d = 0$. $\eta = 0.8554$ and $\eta = 1.083$ are the resonating frequencies when $(\zeta_d)_{opt} = 0.09562$. Massive increments of dynamic responses have occurred at $\zeta_d = \infty$ with a frequency point of $\eta = 0.9713$. The maximum optimal dynamic response of H_∞ optimized TMDI-controlled primary structure determines as 7.3829.

Dynamic response reduction capacity of TMDI and IAVTMD

The variations of optimal dynamic responses of structures controlled by H_2 optimized IAVTMD and TMDI versus frequency ratio with the presence of structural damping ratio; $\zeta_s = 0.01$ have been shown in Figure 14(a). The maximum dynamic responses of structures controlled by H_2 optimized TMDI and IAVTMD are determined as 6.0316 and 5.6129. Therefore, the dynamic response reduction capacity of H_2 optimized IAVTMD is significantly 6.94% superior to H_2 optimized TMDI.

The H_∞ optimized IAVTMD and TMDI controlled structure's dynamic responses are obtained as 6.8385, 5.2456. Accordingly, H_∞ optimized IAVTMD's dynamic response reduction capacity is significantly 23.29% superior to H_∞ optimized TMDI.

Table 3. The optimal design parameters of H_2 and H_∞ optimized TMDI, IAVTMD.

Symbols		H_2 optimization		H_∞ optimization	
TMDI	IAVTMD	TMDI	IAVTMD	TMDI	IAVTMD
ζ_d	ζ_d	0.1313	0.2619	0.096	0.3478
η_d	η_d	1.023	0.5058	1.02	0.5172
$\mu_d + \beta$	$\mu_d + 2\mu_a$	0.06	0.06	0.06	0.06
μ_d	μ_d	0.05	0.04	0.05	0.04
β	μ_a	0.01	0.01	0.01	0.01
—	θ	—	5°	—	5°

Summary and conclusions

The IAVTMD are introduced in this paper. H_2 and H_∞ optimization methods are applied to derive the closed-form expressions for optimal design parameters for IAVTMD and TMDI. The dynamic response reduction capacities of optimum IAVTMD are compared with the dynamic response reduction capacities of optimum conventional TMD and TMDI. The significant outcomes are the following:

1. A higher damper mass ratio, a higher amplifier's mass ratio, and a lower inertial angle are recommended for H_2 and H_∞ optimized IAVTMD for achieving a lower frequency ratio with moderate damping without reducing the static mass of the entire system.
2. The dynamic response capacity of H_2 optimized IAVTMD is significantly 20.87% and 26.47% superior to the dynamic response capacity of H_2 optimized

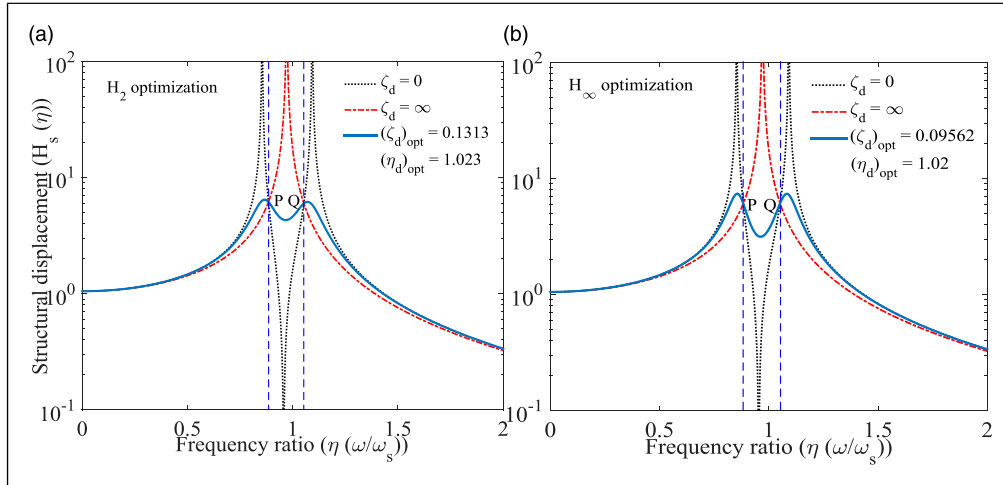


Figure 13. The variations of optimal dynamic responses of structures controlled by (a) H_2 and (b) H_∞ optimized TMDI versus frequency ratio for different values of damping ratio.

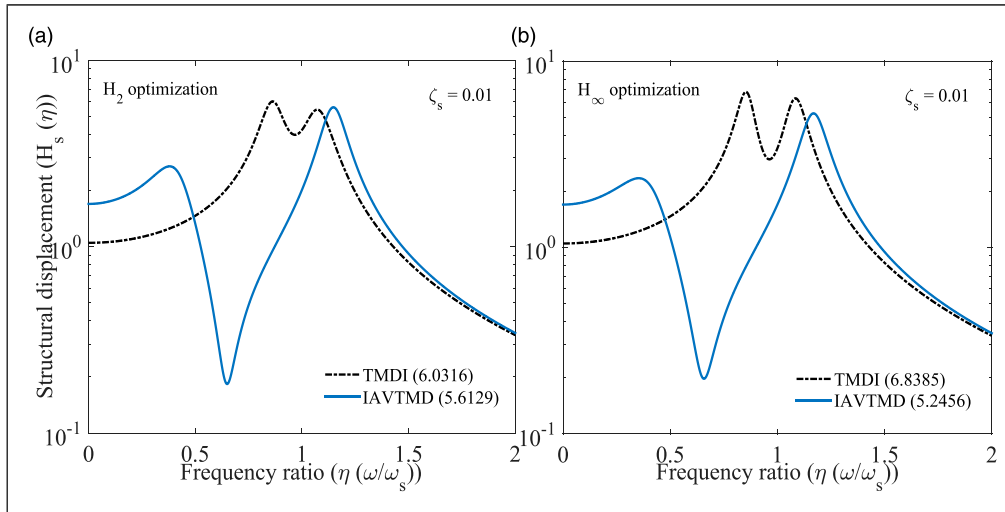


Figure 14. The variations of optimal dynamic responses of structures controlled by (a) H_2 and (b) H_∞ optimized IAVTMD and TMDI versus frequency ratio with the presence of structural damping ratio; $\zeta_s = 0.01$.

conventional tuned mass dampers subjected to harmonic base excitation.

3. The dynamic response capacity of H_∞ optimized IAVTMD is significantly 15.48% superior to the dynamic response capacity of H_∞ optimized conventional tuned mass damper subjected to harmonic base excitation.
4. The dynamic response capacity of H_2 optimized IAVTMD is significantly 33.97% and 47.94% superior to the dynamic response capacity of H_2 optimized conventional tuned mass dampers subjected to random-white noise base excitation.
5. The dynamic response capacity of H_∞ optimized IAVTMD is significantly 33.38% superior to the

dynamic response capacity of H_∞ optimized conventional tuned mass damper subjected to random-white noise base excitation.

6. A higher damper mass ratio and a lower inerter mass ratio are recommended to produce H_2 and H_∞ optimized TMDI with a lower frequency and damping ratio in an affordable range.
7. The dynamic response reduction capacities of H_2 and H_∞ optimized IAVTMD are significantly 6.94% and 23.29% superior to H_2 and H_∞ optimized TMDI.

The paper's main novelty is conceptualizing IAVTMD, TMDI, and the corresponding optimal closed-form solutions. The robust dynamic response capacity of optimum

IAVTMD and TMDI is achieved after applying these closed-form expressions for optimal design parameters. As per the coauthor's suggestions, the applications of IAVTMD and TMDI for multi-degree of freedom systems (MDOF) can be a future research perspective.

Acknowledgements

The authors would like to acknowledge the Inspire faculty grant, grant number DST/INSPIRE/04/2018/000052 for partial financial support for the project. SC would like to acknowledge the MHRD grant received from IIT Delhi during the period of this research work.

Declaration of conflicting interests

The author(s) declared no potential conflicts of interest with respect to the research, authorship, and/or publication of this article.

Funding

The authors would like to acknowledge the Inspire faculty grant, grant number DST/INSPIRE/04/2018/000052 for partial financial support for the project. SC would like to acknowledge the MHRD grant received from IIT Delhi during the period of this research work.

ORCID iDs

Sudip Chowdhury  <https://orcid.org/0000-0001-6218-4843>

Arnab Banerjee  <https://orcid.org/0000-0002-3157-6200>

Sondipon Adhikari  <https://orcid.org/0000-0003-4181-3457>

References

- Adhikari S and Banerjee A (2021) Enhanced low-frequency vibration energy harvesting with inertial amplifiers. *Journal of Intelligent Material Systems and Structures* 33(6): 822–838.
- Adhikari S and Bhattacharya S (2012) Dynamic analysis of wind turbine towers on flexible foundations. *Shock and vibration* 19(1): 37–56.
- Adhikari S, Friswell MI, Litak G, et al. (2016) Design and analysis of vibration energy harvesters based on peak response statistics. *Smart Materials and Structures* 25(6): 065009.
- Asai T, Araki Y and Ikago K (2018) Structural control with tuned inertial mass electromagnetic transducers. *Structural Control and Health Monitoring* 25(2): e2059.
- Baduidana M and Kenfack-Jiotsa A (2021) Optimal design of inerter-based isolators minimizing the compliance and mobility transfer function versus harmonic and random ground acceleration excitation. *Journal of Vibration and control* 27(11–12): 1297–1310.
- Banerjee A, Adhikari S and Hussein MI (2021) Inertial amplification band-gap generation by coupling a levered mass with a locally resonant mass. *International Journal of Mechanical Sciences* 207: 106630.
- Banerjee A, Das R and Calius EP (2019) Waves in structured mediums or metamaterials: a review. *Archives of Computational Methods in Engineering* 26(4): 1029–1058.
- Basili M, De Angelis M and Pietrosanti D (2019) Defective two adjacent single degree of freedom systems linked by spring-dashpot-inerter for vibration control. *Engineering Structures* 188: 480–492.
- Batou A and Adhikari S (2019) Optimal parameters of viscoelastic tuned-mass dampers. *Journal of Sound and Vibration* 445: 17–28.
- Cacciola P, Tombari A and Giaralis A (2020) An inerter-equipped vibrating barrier for noninvasive motion control of seismically excited structures. *Structural Control and Health Monitoring* 27(3): e2474.
- Čakmak D, Tomičević Z, Wolf H, et al. (2022) Stability and performance of supercritical inerter-based active vibration isolation systems. *Journal of Sound and Vibration* 518: 116234.
- Chen MZ and Hu Y (2019a) Analysis for inerter-based vibration system. In: *Inerter and Its Application in Vibration Control Systems*. Berlin, Germany: Springer, pp. 19–39.
- Chen MZ and Hu Y (2019b) *Inerter and its Application in Vibration Control Systems*. Berlin, Germany: Springer.
- Chowdhury S and Banerjee A (2022a) The exact closed-form equations for optimal design parameters of enhanced inerter-based isolation systems. *Journal of Vibration and Control*. Epub ahead of print. DOI: [10.1177/1077546322113342](https://doi.org/10.1177/1077546322113342).
- Chowdhury S and Banerjee A (2022b) The exact closed-form expressions for optimal design parameters of resonating base isolators. *International Journal of Mechanical Sciences* 224: 107284.
- Chowdhury S, Banerjee A and Adhikari S (2021) Enhanced seismic base isolation using inertial amplifiers. *Structures* 33: 1340–1353.
- Chowdhury S, Banerjee A and Adhikari S (2022a) Optimal design of inertial amplifier base isolators for dynamic response control of multi-storey buildings. *International Journal of Structural Stability and Dynamics*. Epub ahead of print. DOI: [10.1142/S0219455423500475](https://doi.org/10.1142/S0219455423500475).
- Chowdhury S, Banerjee A and Adhikari S (2022b) Optimal negative stiffness inertial-amplifier-base-isolators: exact closed-form expressions. *International Journal of Mechanical Sciences* 218: 107044.
- Chowdhury S, Banerjee A and Adhikari S (2023a) The optimal design of dynamic systems with negative stiffness inertial amplifier tuned mass dampers. *Applied Mathematical Modelling* 114: 694–721.
- Chowdhury S, Banerjee A and Adhikari S (2023b) The optimum inertial amplifier tuned mass dampers for nonlinear dynamic systems. *International Journal of Applied Mechanics* 15(2): 2350009. DOI: [10.1142/S1758825123500096](https://doi.org/10.1142/S1758825123500096).
- De Domenico D, Deastra P, Ricciardi G, et al. (2019) Novel fluid inerter based tuned mass dampers for optimised structural control of base-isolated buildings. *Journal of the Franklin Institute* 356(14): 7626–7649.
- De Domenico D and Ricciardi G (2018a) An enhanced base isolation system equipped with optimal tuned mass damper inerter (TMDI). *Earthquake engineering & structural dynamics* 47(5): 1169–1192.
- De Domenico D and Ricciardi G (2018b) Improving the dynamic performance of base-isolated structures via tuned mass damper and inerter devices: a comparative study. *Structural Control and Health Monitoring* 25(10): e2234.

- de Souza Pippi A, Avila SM and Doz G (2022) A review on the use of the inerter device in the structural coupling technique for adjacent building vibration control. In: *Structures*. Amsterdam, Netherlands: Elsevier, Vol. 42, pp. 480–501.
- Den Hartog J and Ormondroyd J (1928) Theory of the dynamic vibration absorber. *ASME Journal of Applied Mechanics* 50(7): 11–22.
- Den Hartog JP (1985) *Mechanical Vibrations*. Chelmsford, MA: Courier Corporation.
- Di Matteo A, Masnata C, Adam C, et al. (2022) Optimal design of tuned liquid column damper inerter for vibration control. *Mechanical Systems and Signal Processing* 167: 108553.
- Frahm H (1909) *Devices for Damping Vibration of Bodies*. US Patent (989958).
- Frandsen NMM, Bilal OR, Jensen JS, et al. (2016) Inertial amplification of continuous structures: large band gaps from small masses. *Journal of Applied Physics* 119(12): 124902.
- Hessabi RM and Mercan O (2016) Investigations of the application of gyro-mass dampers with various types of supplemental dampers for vibration control of building structures. *Engineering Structures* 126: 174–186.
- Hu Y and Chen MZ (2015) Performance evaluation for inerter-based dynamic vibration absorbers. *International Journal of Mechanical Sciences* 99: 297–307.
- Hu Y, Chen MZ, Shu Z, et al. (2015) Analysis and optimisation for inerter-based isolators via fixed-point theory and algebraic solution. *Journal of Sound and Vibration* 346: 17–36.
- Hu Y, Wang J, Chen MZ, et al. (2018) Load mitigation for a barge-type floating offshore wind turbine via inerter-based passive structural control. *Engineering Structures* 177: 198–209.
- Hussein MI, Patrick I, Banerjee A, et al. (2022) Metadamping in inertially amplified metamaterials: Trade-off between spatial attenuation and temporal attenuation. *Journal of Sound and Vibration* 531: 116977.
- Hwang JS, Kim J and Kim YM (2007) Rotational inertia dampers with toggle bracing for vibration control of a building structure. *Engineering Structures* 29(6): 1201–1208.
- Ikago K, Saito K and Inoue N (2012) Seismic control of single-degree-of-freedom structure using tuned viscous mass damper. *Earthquake Engineering & Structural Dynamics* 41(3): 453–474.
- Iwata Y (1982) On the construction of the dynamic vibration absorbers. *Japanese Society of Mechanical Engineering* 820(8): 150–152.
- Javidialesaadi A and Wierschem NE (2018) Optimal design of rotational inertial double tuned mass dampers under random excitation. *Engineering Structures* 165: 412–421.
- Javidialesaadi A and Wierschem NE (2019a) Energy transfer and passive control of single-degree-of-freedom structures using a one-directional rotational inertia viscous damper. *Engineering Structures* 196: 109339.
- Javidialesaadi A and Wierschem NE (2019b) An inerter-enhanced nonlinear energy sink. *Mechanical Systems and Signal Processing* 129: 449–454.
- Jimin H and Zhi-Fang F (2001) *Modal Analysis*. Oxford, UK: Linacre House.
- Kasinos S, Palmeri A, Lombardo M, et al. (2021) A reduced modal subspace approach for damped stochastic dynamic systems. *Computers & Structures* 257: 106651.
- Khodaparast HH, Mottershead JE and Friswell MI (2008) Perturbation methods for the estimation of parameter variability in stochastic model updating. *Mechanical systems and signal processing* 22(8): 1751–1773.
- Krenk S (2005) Frequency analysis of the tuned mass damper. *Journal of Applied Mechanics* 72(6): 936–942.
- Liang R, Wang H, Li J, et al. (2021) Multiple tuned inerter-based dampers for seismic response mitigation of continuous girder bridges. *Soil Dynamics and Earthquake Engineering* 151: 106954.
- Liu C, Chen L, Lee HP, et al. (2022) A review of the inerter and inerter-based vibration isolation: theory, devices, and applications. *Journal of the Franklin Institute* 359(14): 7677–7707.
- Lu L, Xu J, Zhou Y, et al. (2021) Viscous inertial mass damper (VIMD) for seismic responses control of the coupled adjacent buildings. *Engineering Structures* 233: 111876.
- Ma R, Bi K and Hao H (2018) Mitigation of heave response of semi-submersible platform (ssp) using tuned heave plate inerter (THPI). *Engineering Structures* 177: 357–373.
- Ma R, Bi K and Hao H (2021) Inerter-based structural vibration control: a state-of-the-art review. *Engineering Structures* 243: 112655.
- Marian L and Giaralis A (2014) Optimal design of a novel tuned mass-damper–inerter (tmdi) passive vibration control configuration for stochastically support-excited structural systems. *Probabilistic Engineering Mechanics* 38: 156–164.
- Nakaminami S, Kida H, Ikago K, et al. (2017) Dynamic testing of a full-scale hydraulic inerter-damper for the seismic protection of civil structures. In: 7th International Conference on Advances in Experimental Structural Engineering, AESE 2017, Pavia, Italy, 6–8 September 2017. Eucentre, pp. 41–54.
- Nakamura Y, Fukukita A, Tamura K, et al. (2014) Seismic response control using electromagnetic inertial mass dampers. *Earthquake Engineering & Structural Dynamics* 43(4): 507–527.
- Nishihara O and Asami T (2002) Closed-form solutions to the exact optimizations of dynamic vibration absorbers (minimizations of the maximum amplitude magnification factors). *Journal of Vibration and Acoustics* 124(4): 576–582.
- Ormondroyd J (1928) The theory of the dynamic vibration absorber. *Transactions of the ASME, Journal of Applied Mechanics* 50: 9–22.
- Palmeri A and Lombardo M (2011) A new modal correction method for linear structures subjected to deterministic and random loadings. *Computers & structures* 89(11–12): 844–854.
- Petrini F, Giaralis A and Wang Z (2020) Optimal tuned mass-damper–inerter (TMDI) design in wind-excited tall buildings for occupants’ comfort serviceability performance and energy harvesting. *Engineering Structures* 204: 109904.
- Phani AS and Hussein MI (2017) *Dynamics of Lattice Materials*. New York, NY: John Wiley & Sons.
- Pietrosanti D, De Angelis M and Basili M (2017) Optimal design and performance evaluation of systems with tuned mass damper inerter (TMDI). *Earthquake Engineering & Structural Dynamics* 46(8): 1367–1388.
- Pradono MH, Iemura H, Igarashi A, et al. (2008) Application of angular-mass dampers to base-isolated benchmark building. *Structural Control and Health Monitoring* 15(5): 737–745.
- Rana R and Soong T (1998) Parametric study and simplified design of tuned mass dampers. *Engineering structures* 20(3): 193–204.

- Settimi V, Lepidi M and Bacigalupo A (2021) Nonlinear dispersion properties of one-dimensional mechanical metamaterials with inertia amplification. *International Journal of Mechanical Sciences* 201: 106461.
- Shen W, Niyitangamahoro A, Feng Z, et al. (2019) Tuned inerter dampers for civil structures subjected to earthquake ground motions: optimum design and seismic performance. *Engineering Structures* 198: 109470.
- Shen Y, Chen L, Yang X, et al. (2016) Improved design of dynamic vibration absorber by using the inerter and its application in vehicle suspension. *Journal of Sound and Vibration* 361: 148–158.
- Smith MC (2020) The inerter: a retrospective. *Annual Review of Control, Robotics, and Autonomous Systems* 3: 361–391.
- Song J, Bi K, Xu K, et al. (2021) Seismic responses of adjacent bridge structures coupled by tuned inerter damper. *Engineering Structures* 243: 112654.
- Su N, Xia Y and Peng S (2022) Filter-based inerter location dependence analysis approach of tuned mass damper inerter (TMDI) and optimal design. *Engineering Structures* 250: 113459.
- Sun H, Zuo L, Wang X, et al. (2019) Exact h2 optimal solutions to inerter-based isolation systems for building structures. *Structural Control and Health Monitoring* 26(6): e2357.
- Taniker S and Yilmaz C (2013) Phononic gaps induced by inertial amplification in bcc and fcc lattices. *Physics Letters A* 377(31–33): 1930–1936.
- Tiwari ND, Gogoi A, Hazra B, et al. (2021) A shape memory alloy-tuned mass damper inerter system for passive control of linked-sdof structural systems under seismic excitation. *Journal of Sound and Vibration* 494: 115893.
- Wagg DJ (2021) A review of the mechanical inerter: historical context, physical realisations and nonlinear applications. *Nonlinear Dynamics* 104: 13–34.
- Wang FC, Yu CH, Chang ML, et al. (2006) The performance improvements of train suspension systems with inerters. In: Proceedings of the 45th IEEE Conference on Decision and Control, San Diego, CA, 13–15 December 2006. IEEE, pp. 1472–1477.
- Wang H, Gao H, Li J, et al. (2021) Optimum design and performance evaluation of the tuned inerter-negative-stiffness damper for seismic protection of single-degree-of-freedom structures. *International Journal of Mechanical Sciences* 212: 106805.
- Wang M and Sun F (2018) Displacement reduction effect and simplified evaluation method for sdof systems using a clutching inerter damper. *Earthquake Engineering & Structural Dynamics* 47(7): 1651–1672.
- Warburton GB (1982) Optimum absorber parameters for various combinations of response and excitation parameters. *Earthquake Engineering & Structural Dynamics* 10(3): 381–401.
- Yang J, Jiang JZ and Neild SA (2020) Dynamic analysis and performance evaluation of nonlinear inerter-based vibration isolators. *Nonlinear Dynamics* 99(3): 1823–1839.
- Yilmaz C and Hulbert G (2010) Theory of phononic gaps induced by inertial amplification in finite structures. *Physics Letters A* 374(34): 3576–3584.
- Yilmaz C, Hulbert GM and Kikuchi N (2007) Phononic band gaps induced by inertial amplification in periodic media. *Physical Review B* 76(5): 054309.
- Zhang R, Zhao Z and Dai K (2019) Seismic response mitigation of a wind turbine tower using a tuned parallel inerter mass system. *Engineering Structures* 180: 29–39.
- Zhang Z and Fitzgerald B (2020) Tuned mass-damper-inerter (TMDI) for suppressing edgewise vibrations of wind turbine blades. *Engineering Structures* 221: 110928.
- Zhang Z and Høeg C (2021) Inerter-enhanced tuned mass damper for vibration damping of floating offshore wind turbines. *Ocean Engineering* 223: 108663.
- Zhao Z, Zhang R, Jiang Y, et al. (2019a) Seismic response mitigation of structures with a friction pendulum inerter system. *Engineering Structures* 193: 110–120.
- Zhao Z, Zhang R, Jiang Y, et al. (2019b) A tuned liquid inerter system for vibration control. *International Journal of Mechanical Sciences* 164: 105171.
- Zilletti M, Elliott SJ and Rustighi E (2012) Optimisation of dynamic vibration absorbers to minimise kinetic energy and maximise internal power dissipation. *Journal of sound and vibration* 331(18): 4093–4100.